Novel Hyperelastic Models for Large Volumetric Deformations

Kevin M. Moerman[a,b,**], Behrooz Fereidoonnezhad[a], Patrick McGarry[a,*]

[a]*National University of Ireland Galway, Galway, Ireland*
[b]*Massachusetts Institute of Technology, Cambridge, MA, United States of America*

Abstract

Materials such as elastomeric foams, lattices, and cellular solids are capable of undergoing large elastic volume changes. Although many hyperelastic constitutive formulations have been proposed for deviatoric (shape changing) behaviour, few variations exist for large deformation volumetric behaviour. The first section of this paper presents a critical analysis of current volumetric hyperelastic models and highlights their limitations for large volumetric strains. In the second section of the paper we propose three novel volumetric strain energy density functions, which: 1) are valid for large volumetric deformations, 2) offer separate control of the volumetric strain stiffening behaviour during shrinkage (volume reduction) and expansion (volume increase), and 3) provide precise control of non-monotonic volumetric strain stiffening. To illustrate the ability of the novel formulations to capture complex volumetric material behaviour they are fitted and compared to a range of published experimental data.

Keywords: Hyperelasticity, Volumetric Deformation, Finite Strain, Strain Energy Density, Shrinkage, Expansion

*Corresponding author
**Corresponding author
Email addresses: kevin.moerman@nuigalway.ie (Kevin M. Moerman), patrick.mcgarry@nuigalway.ie (Patrick McGarry)

1. Introduction

Foams, lattices, and cellular materials are common in nature and engineering applications [1, 2, 3, 4]. Given the large elastic volume changes these materials can undergo [5], accurate descriptions of material behaviour beyond the small strain domain is required. Such behaviour may include an asymmetric shrinkage-expansion response in addition to a highly non-linear pressure-volume relationship.

Hyperelastic continuum models offer a convenient means to model the large strain mechanical behaviour of complex materials. However, although the hyperelasticity literature is rich in terms of variations in modelling of the deviatoric (shape changing) material response, as evident from the many different formulations which have been proposed (e.g. close to a hundred described in a recent review [6]), few variations exist for modelling the volumetric contribution (e.g. [7, 8, 9, 10]).

The goal of this study is to provide novel volumetric strain energy formulations which: 1) are valid for large volumetric deformations, and 2) enable the separate control of volumetric strain-dependent stiffening during shrinkage (volume reduction), and expansion (volume increase).

Accurate modelling of the volumetric behaviour of materials like soft foams and lattices is of interest since it is relevant to the design of support structures (see review [11]), such as foam cushions and seats [12, 13, 14, 15], helmets [16], and shoes and insoles ([17, 18, 19]). Furthermore compliant lattices and foams are also employed in the design of soft robotics [20, 21, 22, 23]. Recent advances in material science include the development of ceramic nanolattices [24], mycelium-based bio-foams [25], ultraporous sponges [26] graphene foams and aerogels (e.g [27, 28, 29, 30]) some capable of recovering from 90% compression [31]. Furthermore, accurate volumetric formulations are relevant to stroke biomechanics research since blood clot contractions cause large volume changes (e.g. possibly over 80% volume loss [32]).

Hyperelastic constitutive formulations have their origins in the modelling of rubber [33, 34, 35, 36]. Although rubber is most commonly modelled as incompressible (no volume change), it does present with a non-linear pressure-volume response during large deformation hydrostatic compression (20% volume reduction [36]), and volumetric hyperelastic formulations capturing this behaviour have been proposed (e.g. [7]). These, as we will show here, are however not generally valid for very large hydrostatic compression.

Hyperelasticity is also commonly used for soft tissues (see review [6]).

However, like with rubbers, these are often assumed to be incompressible or nearly-incompressible. For these applications the volumetric contributions are commonly considered largely as a simple penalty term to enforce (near) incompressibility (e.g. [37, 38]), rather than a topic of detailed investigation. Consequently the formulations used for these volumetric contributions are often not valid for very large volume changes. For foams and highly compressible materials the so called hyperfoam formulation [8, 39, 40]) is common (see for instance [41, 17, 42, 43, 44, 14]). However, we show here it is not robustly designed for very large volume changes.

The first part of this study is a critical analysis of current volumetric hyperelastic formulations, and presents a discussion of their limitations for large volumetric deformations and non-linear applications. In the second part of this study three novel volumetric strain energy formulations are presented (and several variations in the appendix) which offer validity for large volumetric strains as well as flexibility for experimental fitting of complex behaviour for both the shrinkage and expansion domain. In addition, the third formulation was expanded to include non-monotonic volumetric strain stiffening (e.g. potentially leading to a plateau in the observed stress) as seen for crushable foams and cellular materials. Finally, the models are compared to experimental data for neoprene rubber foam [45], flexible open-cell polyurethane cushioning foam [17], natural cork [46], and rigid closed-cell polyurethane foam [47].

2. Theoretical background and rationale

In hyperelasticity the constitutive behaviour, i.e. the material's stress-strain behaviour, is derived from a formulated strain energy density (SED) function (for a more detailed discussion of these concepts the reader is referred to established text-books on the subject [48] and [35]). In the case of uncoupled formulations the strain energy consists of additive deviatoric (shape changing) $\Psi_{dev}(\tilde{\mathbf{C}})$ and volumetric (volume changing) $\Psi_{vol}(J)$ contributions:

$$\Psi(\tilde{\mathbf{C}}, J) = \Psi_{dev}(\tilde{\mathbf{C}}) + \Psi_{vol}(J) \tag{1}$$

Here $\tilde{\mathbf{C}}$ and J represent the deviatoric right Cauchy-Green tensor and the volume ratio (or Jacobian), respectively. The Cauchy stress for this formulation can be written:

$$\boldsymbol{\sigma} = \boldsymbol{\sigma}_{\boldsymbol{dev}} + \sigma_h \mathbf{I} \tag{2}$$

where $\boldsymbol{\sigma_{dev}}$ is the deviatoric stress tensor, σ_h is the scalar hydrostatic stress, and $\mathbf{I}$ is the identity tensor. σ_h is given as

$$\sigma_h = \frac{1}{3}\,\mathrm{tr}(\boldsymbol{\sigma}) = -p \tag{3}$$

where $p = -\sigma_h$ is commonly referred to as the pressure. For an un-coupled formulation, σ_h is determined from the volumetric component of the strain energy density, such that

$$\sigma_h = \frac{\partial \Psi_{vol}(J)}{\partial J} \tag{4}$$

This paper focuses on the analysis and development of volumetric strain energy density formulations for large volumetric deformations. We consider both volume reduction ($J < 1$) and volume increase ($J > 1$), referred to as *shrinkage* and *expansion*, respectively.

Although many formulations have been proposed for deviatoric strain energy contributions Ψ_{dev} (see for instance the review article [6]), relatively few formulations have been proposed for the volumetric strain energy contributions $\Psi_{vol}(J)$ (for a more detailed discussion of volumetric strain energy formulations the reader is referred to the surveys by Doll and Schweizerhof [10] and Horgan and Murphy [49]). Moreover, volumetric components of hyperelastic models are not typically subjected to rigorous analysis in order to ensure that physically realistic behaviour for large volume changes is maintained. The study of Doll and Schweizerhof [10] establishes 9 criteria (summarised as *I*-*IX* in Table 1) that should be satisfied in order to ensure physically realistic material behavior during expansion and shrinkage. Here we add a tenth (*X* in Table 1), namely: the volumetric component of a hyperelastic model should be capable of precisely describing strain stiffening for all values of J (shrinkage and expansion).

Table 1: Physical constraints and criteria for $\Psi_{vol}(J)$

id	**Description**	**Form**
I	Zero SED in reference state	$\Psi_{vol}(J=1)=0$
II	Zero hydrostatic stress in reference state	$\sigma_h(J=1)=0$
III	Positive strain energy density	$\Psi_{vol}(J\neq 1)>0$
IV	Consistent with linear elasticity	$\frac{d^2\psi_{vol}(J=1)}{dJ^2}=\kappa$
V	SED approaches ∞ if J approaches 0	$\lim_{J\to 0}\Psi_{vol}(J)=\infty$
VI	Hydrostatic stress approaches $-\infty$ if J approaches 0	$\lim_{J\to 0}\sigma_h(J)=-\infty$
VII	SED approaches ∞ if J approaches ∞	$\lim_{J\to \infty}\Psi_{vol}(J)=\infty$
VIII	Hydrostatic stress approaches ∞ if J approaches ∞	$\lim_{J\to \infty}\sigma_h(J)=\infty$
IX	Tangent modulus >0 (polyconvexity)	$\frac{d^2\psi_{vol}(J)}{dJ^2}\geq 0$
X	Control of strain stiffening for all J	

2.1. Structure of this paper

The current paper is structured as follows.

In Section 3 we analyze the capability of four existing models to satisfy the criteria set out in Table 1:

- In Section 3.1 commonly implemented single parameter models are analysed;
- In Section 3.2 the formulation by Bischoff et al. [7] for hydrostatic compression of rubber is analysed;
- In Section 3.3 we analyse the modified Ogden formulation [9, 50], a simplified form of which has been implemented in ABAQUS® (2018, Dassault Systèmes Simulia Corp.);
- In Section 3.4 we analyse the Ogden-Hill hyperfoam formulation [8], which has been implemented in ABAQUS®, for highly compressible elastomers;
- In Section 3.5 we analyze a model by Doll and Schweizerhof [10].
- In Section 3.6 we analyze the model by Montella et al. [51].

In Section 4 we propose three novel formulations that improve upon existing formulations in terms of the criteria outlined in Table 1:

- In Section 4.1 we expand the single parameter model (of Equation 6) to fulfil all criteria of Table 1, and to provide independent control of strain stiffening in shrinkage and expansion;

- In Section 4.2 we present a formulation that facilitates precise prescription of "lock-up" strains in expansion and shrinkage;

- In Section 4.3 we expand the model presented in Section 4.2 to also capture non-monotonic strain stiffening (typically observed in elastomeric foams).

This paper focuses on volumetric strain energy density formulations for large volumetric deformations. Properties of several commonly used forms are discussed and three novel formulations are proposed. Although the arguments are most readily presented using uncoupled formulations, they can be extended to coupled formulations where the effective volumetric response can also be separately identified.

All visualizations presented here were created based on the free and open source MATLAB® (R2019b, The MathWorks Inc., Natick, MA, USA) toolbox GIBBON (https://www.gibboncode.org, [52, 53]). Readers interested in exploring MATLAB® implementations, and associated visualizations, of all discussed formulations presented here, may explore the following demo which was added to GIBBON as part of this study: `DEMO_volumetric_SED_eval.m`.

3. Review and critical analysis of current volumetric SED formulations

3.1. Common single parameter volumetric SED formulations

Two commonly used forms for $\Psi_{vol}(J)$, in particular for uncoupled formulations, are (e.g. [54]):

$$\Psi_{vol}(J) = \frac{\kappa}{2}\ln(J)^2 \tag{5}$$

and (e.g. [55, 56]):

$$\Psi_{vol}(J) = \frac{\kappa}{2}(J-1)^2 \tag{6}$$

These are featured in many finite element implementations such as the open source package FEBio [57] and the proprietary software ABAQUS®.

These formulations have largely been used to model materials that are assumed to be nearly incompressible (such as rubbers and soft tissues), for which $J \approx 1$. The motivation for these formulations stems largely from their mathematical convenience. Although their performance when $J \approx 1$ is valid, as we shall describe shortly, non-physical behaviour occurs for large volume changes. Table 1 lists several validity criteria and physical constraints (see also [10, 35]) for volumetric strain energy density formulations. Doll and Schweizerhof [10] examined common formulations and showed that equation 5 does not conform to criteria *VIII* (for high expansions the stress approaches 0 rather than ∞) and criteria *IX* (for expansion the stiffness reduces to zero at $J = e \approx 2.718$ after which it becomes negative for $J > e$). These effects are summarised in Figure 1.

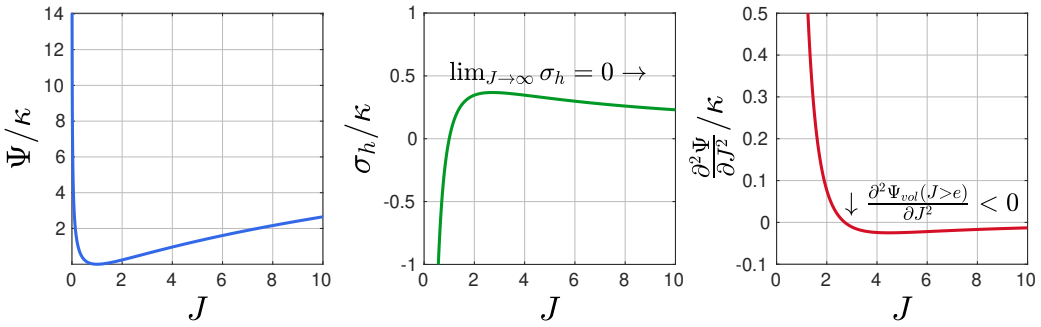

Figure 1: The normalized strain energy density (left), hydrostatic stress (middle), and tangent modulus (right), for the formulation of equation 5

Furthermore it was demonstrated that equation 6 does not conform to criteria *V* (for high shrinkage Ψ_{vol} approaches $\kappa/2$ rather than ∞) and criteria *VI* of Table 1 (for high shrinkage σ_h approaches $-\kappa$ rather than $-\infty$). These effects are summarised in Figure 2.

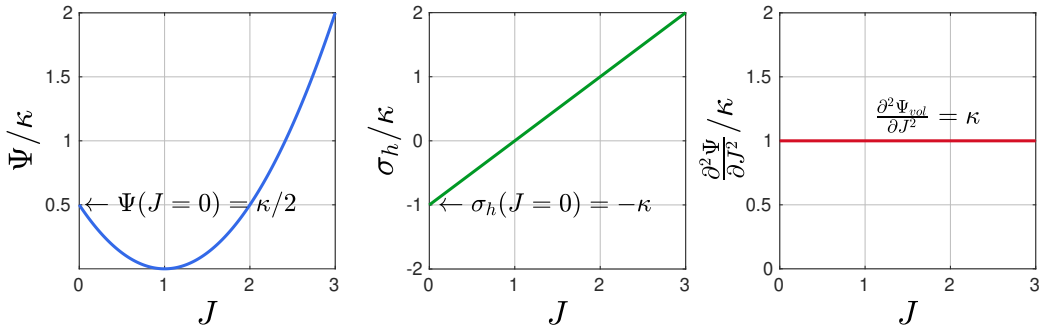

Figure 2: The normalized strain energy density (left), hydrostatic stress (middle), and tangent modulus (right), for the formulation of equation 6

For incompressible materials the problems outlined above are largely avoided provided that the conditions that $J \approx 1$ can be numerically enforced with sufficient precision. However, when modelling of compressible material behaviour is of interest, the criteria outlined in Table 1 must be satisfied. Finally, these formulations exhibit one fixed type of strain dependent behaviour and asymmetry in terms of the difference between shrinkage and expansion, and therefore these formulations do not conform to criteria X of Table 1.

3.2. The Bischoff formulation

Bischoff et al. [7] presents what can be considered a higher-order representation of equation 6:

$$\Psi_{vol}(J) = \frac{\kappa}{\alpha^2}\Big(\cosh\big(\alpha(J-1)\big) - 1\Big) = \kappa\sum_{m=1}^{\infty}\frac{\alpha^{2(m-1)}}{(2m)!}(J-1)^{2m} \qquad (7)$$

Where α is an additional material parameter. Bischoff et al. [7] demonstrates a good fit to the experimental hydrostatic compression data for rubber up to 20%. However, this formulation, and related polynomial forms, have the same pitfalls as the form of equation 6, i.e. they present with a finite strain energy, and hydrostatic stress for $J = 0$, thereby violating criteria V and VI of Table 1. Furthermore, this formulation does not offer independent control of the behaviour for shrinkage and expansion, and therefore criteria X of Table 1 is not met.

3.3. The modified Ogden formulation

The modified Ogden formulation [50, 9] is given by:

$$\Psi_{vol}(J) = \frac{\kappa}{\beta^2}\left(J^{-\beta} - 1 + \beta \ln(J)\right) \tag{8}$$

, with κ the bulk modulus and β (with $\beta \neq 0$) a material parameter controlling the degree of non-linearity. The hydrostatic stress can be derived as:

$$\sigma_h(J) = \frac{\kappa}{\beta J}(1 - J^{-\beta}) \tag{9}$$

and the tangent modulus:

$$\frac{\partial^2 \Psi}{\partial J^2} = \frac{\kappa}{\beta J^2}\left((\beta + 1)J^{-\beta} - 1\right) \tag{10}$$

Figure 3 below illustrates the behaviour of this formulation for shrinkage and expansion and for a range of positive and negative β values. In Ogden [9] the formulation is presented in relation to volume reductions only, and with $\beta > 0$. However, these restrictions are not generally enforced, and if $\beta = -2$ is chosen this formulation reduces to the volumetric contribution, implemented in ABAQUS®, for the uncoupled Aruda-Boyce [58] and Van der Waals [59, 60] formulations. For shrinkage this formulation presents with suitable behaviour. For this domain increasing β results in an increase in strain stiffening. Reducing β has the opposite effect with severely negative values even inducing a stiffness reduction and a plateauing behaviour (e.g. see graph for $\beta = -15$ in Figure 3). By studying equation 8 and Figure 3 it becomes clear this formulation does not conform to all criteria of Table 1 in the expansion domain. Specifically if $\beta \geq -1$ the tangent tends to zero (i.e. $\lim_{J\to\infty} \frac{d^2\psi_{vol}(J)}{dJ^2} = 0$), and negative tangents occur if $\beta > -1$ (e.g. see graphs for $\beta = 2$ and $\beta = 15$ in Figure 3), thereby violating criteria *VII*, *VIII* and *IX*. Furthermore, since this formulation does not offer independent control over the response for shrinkage and expansion, it does not conform to criteria *X* of Table 1.

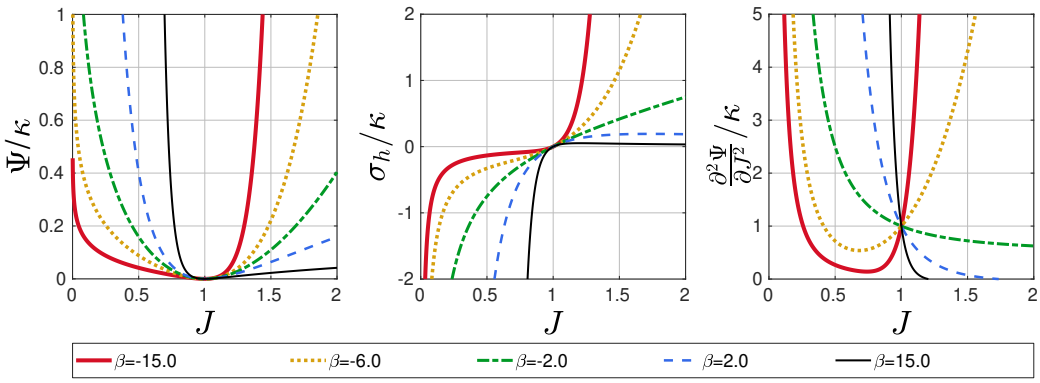

Figure 3: The normalized strain energy density (left), hydrostatic stress (middle), and tangent modulus (right), for the modified Ogden formulation (equation 8). Curves drawn for $\kappa = 1$, and $\beta = [-15, 15]$

3.4. The hyperfoam formulation

A popular (see for instance [41, 17, 42, 43, 44, 14]) formulation for modelling of highly compressible materials is the so called Ogden-Hill or *hyperfoam* material implemented in ABAQUS®. The formulation, (see [8], [39] page 48, and developments in [40]) is given by:

$$\Psi(\lambda_1, \lambda_2, \lambda_3, J) = \sum_{a=1}^{N} \frac{2\mu_a}{\alpha_a^2}\left(\lambda_1^{\alpha_a} + \lambda_2^{\alpha_a} + \lambda_3^{\alpha_a} - 3 + \frac{1}{\beta_a}(J^{-\alpha_a\beta_a} - 1)\right) \quad (11)$$

Here μ_a and α_a are Ogden-like [35, 9] hyperelastic parameters, and β_a enables additional enhancement of volumetric contributions.

To review the properties of this formulation we restrict ourselves to a first order formulation ($N = 1$). Furthermore, for volumetric deformations, one may use the conditions $\lambda_1 = \lambda_2 = \lambda_3 = J^{-\frac{1}{3}}$, reducing equation 11 to:

$$\Psi(J) = \frac{2\mu}{\alpha^2}\left(3(J^{\frac{\alpha}{3}} - 1) + \frac{1}{\beta}(J^{-\alpha\beta} - 1)\right) \quad (12)$$

The bulk modulus for this formulation is derived from:

$$\kappa = \mu\left(\beta + \frac{1}{3}\right) \quad (13)$$

Therefore, to ensure $\kappa > 0$ one obtains the constraint $\beta > -\frac{1}{3}$. Furthermore, from equation 11, it is clear that $\beta_a \neq 0$ is also a constraint. From equation

12 the hydrostatic stress can be derived as:

$$\sigma_h(J) = J^{-1}\frac{2\mu}{\alpha}(J^{\frac{\alpha}{3}} - J^{-\alpha\beta}) \tag{14}$$

and the tangent modulus:

$$\frac{\partial^2\Psi}{\partial J^2} = J^{-2}\frac{2\mu}{\alpha}\left((\frac{\alpha}{3} - 1)J^{\frac{\alpha}{3}} + (\alpha\beta + 1)J^{-\alpha\beta}\right) \tag{15}$$

Although this formulation is reported to be valid in the domain $-\frac{1}{3} < \beta < 0$ several issues were revealed in this study. As shown in Figure 4, in this domain one encounters a reduction in the tangent modulus eventually creating negative volumetric stiffness. Furthermore, the stress may reduce to 0 as $J = 0$ is approached. It was found that the effect is exacerbated by the parameter α, therefore even if a negative β is chosen close to 0 (which appears to provide valid behaviour in Figure 4) a negative stiffness may still occur if the α parameter is sufficiently high.

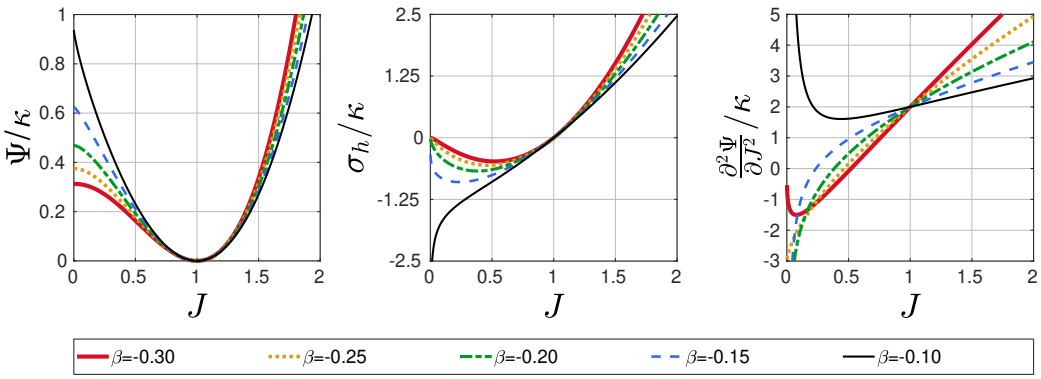

Figure 4: The normalized strain energy density (left), hydrostatic stress (middle), and tangent modulus (right), for the hyperfoam formulation. Curves drawn for $\mu = 1$, $\alpha = 8$, and $\beta = [-0.3, -0.1]$

The illustrated behaviour for the domain $-\frac{1}{3} < \beta < 0$ when $\alpha > 0$ would lead one to add the constraint $\beta > 0$ for this formulation. Figure 5 explores the effect of varying α when $\beta > 0$. In terms of the tangent modulus it may be seen to decay, become constant, or become negative. The hydrostatic stress for $\alpha \leq 6$ is seen to reach a maximum and become constant or reduced with increasing J (due to negative stiffness). It was found that a negative

tangent modulus may occur when $0 < \alpha \leq 6$ (see expansion domain for the graphs for $\alpha \leq 6$). Hence to avoid this it appears that $\alpha > 6$ is an additional constraint to avoid a negative tangent modulus if $\beta > 0$.

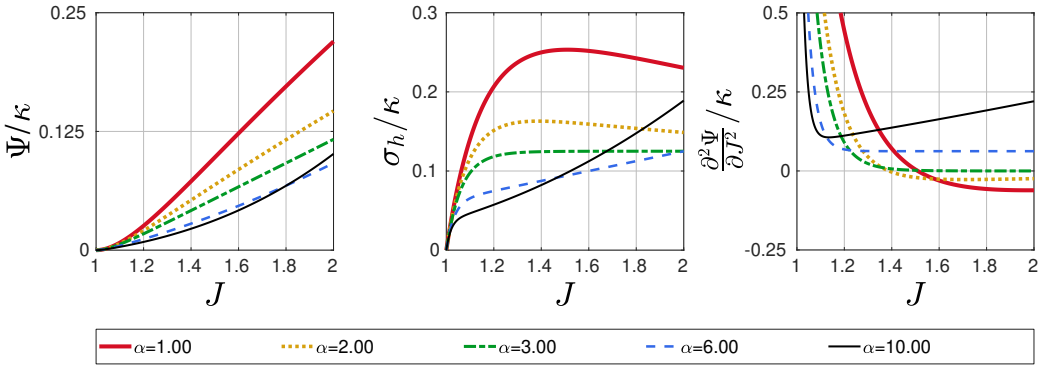

Figure 5: The normalized strain energy density (left), hydrostatic stress (middle), and tangent modulus (right), for the hyperfoam formulation. Curves drawn for $J = [1, 2]$, $\mu = 1$, $\beta = 5$, and $\alpha = [1, 10]$

Figure 6 presents the effect of varying β (when $\beta > 0$) when $\alpha > 6$ ($\alpha = 8$). It is clear that a positive β value enhances the shrinkage domain while suppressing the expansion domain.

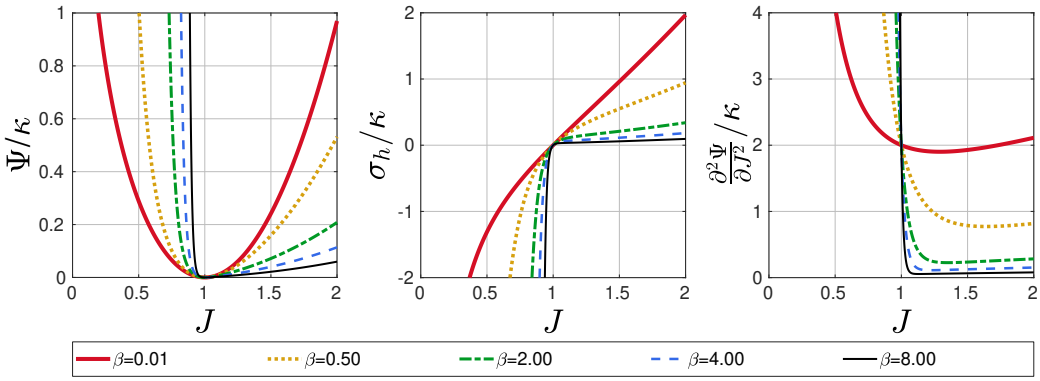

Figure 6: The normalized strain energy density (left), hydrostatic stress (middle), and tangent modulus (right), for the hyperfoam formulation. Curves drawn for $\mu = 1$, $\alpha = 8$, and $\beta = [0.01, 8]$

Figure 7 is similar to Figure 6 except now a negative α is explored ($\alpha = -8$). These graphs show that now β changes its role to instead enhance the

expansion domain while suppressing the shrinkage domain. Furthermore, it was observed that a negative tangent modulus may occur if β is close to zero (see graph for $\beta = 0.01$).

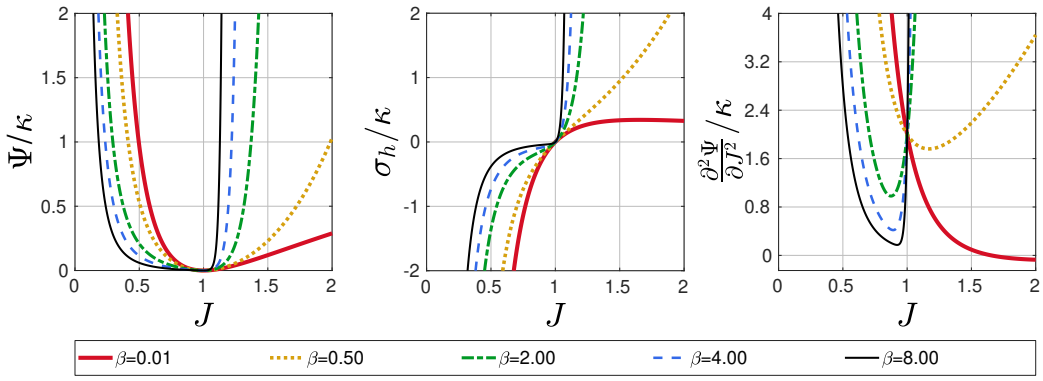

Figure 7: The normalized strain energy density (left), hydrostatic stress (middle), and tangent modulus (right), for the hyperfoam formulation. Curves drawn for $\mu = 1$, $\alpha = -8$, and $\beta = [0.01, 8]$

In summary, in the above analysis, several additional constraints have been identified for the hyperfoam formulation. It appears $\beta > 0$ is a constraint. In addition, if a positive α parameter is used, $\alpha > 6$ appears a requirement. If instead negative α values are employed a negative tangent modulus might occur for β values close to 0. It is therefore concluded that the hyperfoam formulation is highly constrained in terms of the choice of β and α.

For conventional Ogden hyperelastic formulations (see [35]) the parameter α usually controls the degree of non-linarity (or strain hardening) predominantly for the deviatoric behaviour, and for fitting, positive or negative α parameters may required. However, as demonstrated here, for this Ogden-like hyperfoam formulation, α not only strongly influences the volumetric behaviour, it also changes the role of β (from enhancing shrinkage to enhancing expansion) when it changes sign. Furthermore, the suggested constraint $\alpha > 6$ (for $\alpha > 0$) may impose a potentially undesirable degree of non-linearity on the deviatoric response. For instance, some materials may demonstrate little strain stiffening such that they require $\alpha < 6$ (this includes Neo-Hookean behaviour, which requires $\alpha = 2$). Finally, even if suitable constraints are implemented, this formulation does not offer independent control in terms of enhancement for the shrinkage and expansion

domains, it therefore does not satisfy criteria X of Table 1.

3.5. The Doll and Schweizerhof [10] formulation

Doll and Schweizerhof [10] proposed the following volumetric strain energy density formulation:

$$\Psi_{vol}(J) = \frac{\kappa}{\alpha+\beta}\left(\frac{1}{\alpha+1}J^{\alpha+1} + \frac{1}{\beta-1}J^{-(\beta-1)}\right) - \frac{\kappa}{(\alpha+1)(\beta-1)} \tag{16}$$

with the material parameter constraints: $\alpha > 0$ and $\beta > 1$. Besides satisfying all criteria listed in Table 1, this formulation also offers some control over the response in shrinkage and expansion. Furthermore, by choosing $\alpha = \beta$ the pressure symmetry $p(J) = -p(\frac{1}{J})$ is obtained, and by using $\beta = \alpha + 2$ one obtains symmetry in terms of strain energy, i.e. $\Psi(J) = \Psi(\frac{1}{J})$. Figure 8 illustrates the effect of the parameter α. It enhances the response for expansion while mildly suppressing the response for shrinkage.

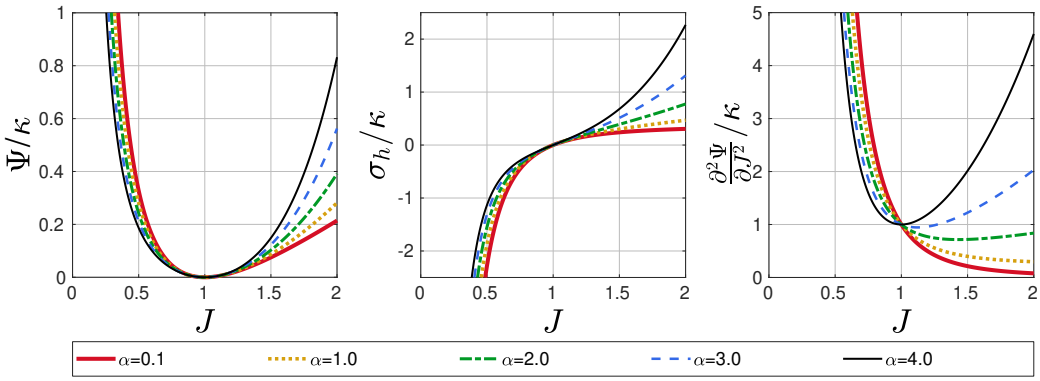

Figure 8: The normalized strain energy density (left), hydrostatic stress (middle), and tangent modulus (right), for the Doll and Schweizerhof [10] formulation. Curves drawn for $\kappa = 1$, $\beta = 3$, and $\alpha = [0.1, 4]$

The parameter β has the opposite effect, as Figure 9 shows, since it enhances the response for shrinkage while suppressing the response in expansion.

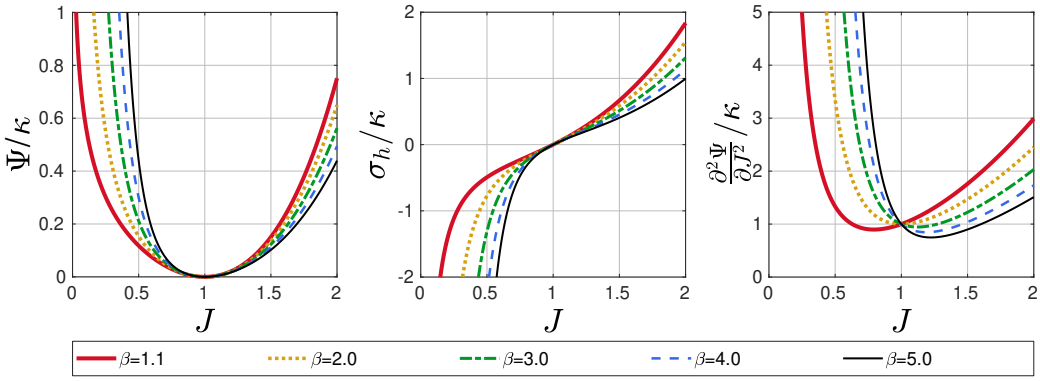

Figure 9: The normalized strain energy density (left), hydrostatic stress (middle), and tangent modulus (right), for the Doll and Schweizerhof [10] formulation. Curves drawn for $\kappa = 1$, $\alpha = 3$, and $\beta = [1.1, 5]$

Although this formulation offers a way to control the response for shrinkage and expansion through the parameters α and β, both parameters have an effect on both domains. Therefore, since the control is not independent, criteria X of Table 1 is not fully met.

Furthermore, it is noted here that this formulation has the property that the minimum stiffness state need not be at $J = 1$ (see location of minima in the image on the right of Figure 9). Although this is in principle not invalid, it may not be realistic or desirable.

3.6. The Montella et al. [51] formulation

Montella et al. [51] proposed the following volumetric strain energy density formulation:

$$\Psi_{vol}(J) = \frac{\kappa}{2\beta_1} e^{\beta \ln(J)^2} + \frac{\kappa_2}{m\beta_2} e^{\beta_2 |\ln(J)|^m} \tag{17}$$

Note that it is presented here by making use of $\mathrm{tr}\big(\ln(\mathbf{U})\big) = \ln\big(\det(\mathbf{U})\big) = \ln(J)$, with $\mathbf{U} = \sqrt{\mathbf{C}}$ the right stretch tensor. To conform to criteria I of Table 1 (zero strain in the reference state) the following trivial modification can be made:

$$\Psi_{vol}(J) = \frac{\kappa}{2\beta_1}\big(e^{\beta_1 \ln(J)^2} - 1\big) + \frac{\kappa_2}{m\beta_2}\big(e^{\beta_2 |\ln(J)|^m} - 1\big) \tag{18}$$

Here κ is the bulk modulus, and κ_2 is referred to as the large strain bulk modulus. The parameters β_1 and β_2, are dimensionless and have the constraints $\beta_1 \geq \frac{1}{8}$ and $\beta_2 \geq \frac{1}{8}$.

Figure 10 illustrates the effect of varying the parameter β_1 and includes the lower limit $\beta_1 = \frac{1}{8}$. This parameter β_1 is seen to allow for the simultaneous variation of response for shrinkage and expansion. The parameter β_2 has a similar effect in the second term of equation 18. The parameter κ_2 offers added control of the slope for higher strains.

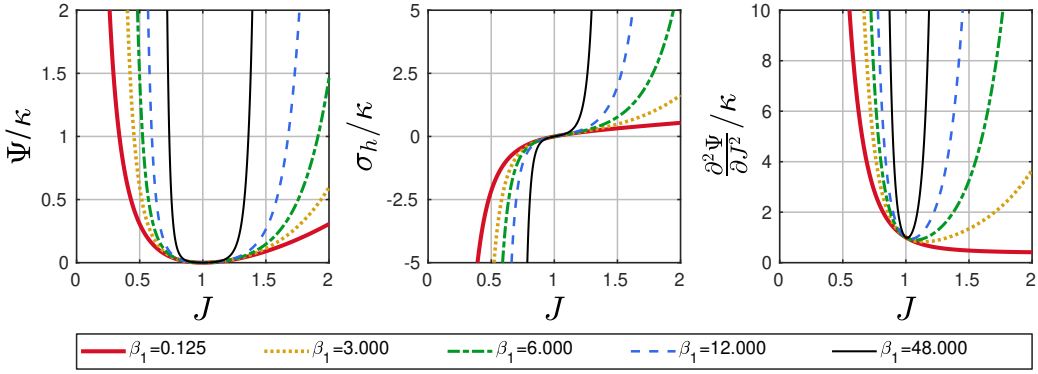

Figure 10: The normalized strain energy density (left), hydrostatic stress (middle), and tangent modulus (right), for the Montella et al. [51] formulation. Curves drawn for $\kappa = 1$, $\kappa_2 = 1$, $\beta_2 = \frac{1}{8}$, $m = 4$, and $\beta_1 = [\frac{1}{8}, 48$

Figure 11 illustrates the effect of varying the parameter m. The parameter m can be seen the enhance the response for $J > e$, and $J < \frac{1}{e}$ and to suppress the response in the range $\frac{1}{e} < J < e$. This suppressing/enhancing effect results in the ability to a plateau region for the expansion domain. If $m > 2$ the second term vanishes for $J = 1$ hence this appears to be a constraint on m if criteria IV of Table 1 is to be respected. However, in this study $m \geq 4$ appeared a requirement since discontinuities were observed for the tangent modulus when $J \approx 1$ and if $2 < m < 4$ (see for example the curve for $m = 2.1$ in Figure 11).

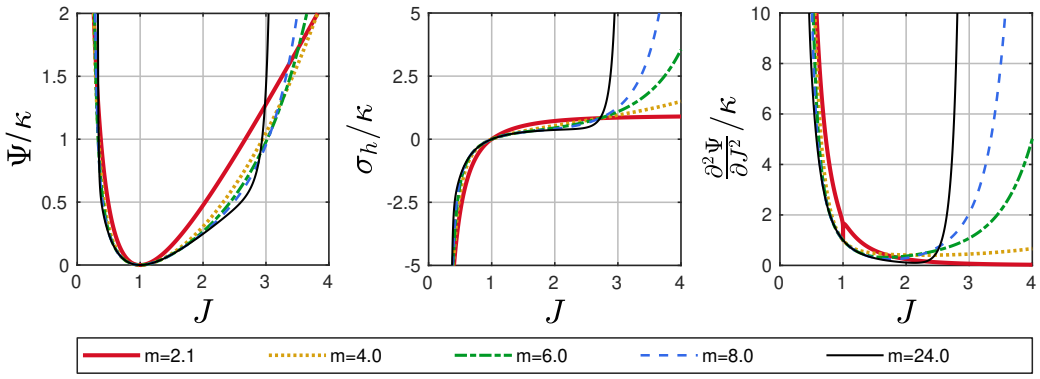

Figure 11: The normalized strain energy density (left), hydrostatic stress (middle), and tangent modulus (right), for the Montella et al. [51] formulation. Curves drawn for $\kappa = 1$, $\kappa_2 = 1$, $\beta_2 = \frac{1}{8}$, $\beta_1 = \frac{1}{8}$, and $m = [2.124]$

The Montella et al. [51] formulation of equation 18 offers a flexible formulation for modelling of large strain volumetric deformations. Further more, provided the constraints described are respected, the formulation conforms to criteria *I-IX* of Table 1. However, this formulation does not offer independent control of the response for shrinkage and expansion.

4. The proposed volumetric strain energy density formulations

Three novel volumetric strain energy densities are presented in this section which offer separate control over the strain dependent behaviour for shrinkage and expansion.

4.1. Formulation 1

The first formulation is inspired by equation 6. A power was added to the volume ratio to enable control of the degree of strain stiffening. Next two terms were created such that one features a positive power and one a negative power, the former being most sensitive to expansion while the latter is most sensitive to shrinkage, leading to:

$$\Psi_{vol}(J) = \frac{\kappa}{4}\left(\frac{1}{{\beta_1}^2}(J^{\beta_1} - 1)^2 + \frac{1}{{\beta_2}^2}(J^{-\beta_2} - 1)^2\right) \tag{19}$$

Besides the bulk modulus κ, this formulation features the material parameters β_1 and β_2, which control the degree of strain stiffening in terms of expansion and shrinkage respectively, with $\kappa \in \mathbb{R}_{>0}$, $\beta_1 \in \mathbb{R}_{>2}$, and $\beta_2 \in \mathbb{R}_{>0}$.

The hydrostatic stress for this formulation is:

$$\sigma_h(J) = \frac{\kappa}{2J}\left(\frac{1}{\beta_1}(J^{2\beta_1} - J^{\beta_1}) - \frac{1}{\beta_2}(J^{-2\beta_2} - J^{-\beta_2})\right) \tag{20}$$

and the tangent modulus:

$$\begin{aligned}\frac{\partial^2 \Psi_{vol}(J)}{\partial J^2} = \frac{\kappa}{2J^2}\Bigg[&\left((2 - \frac{1}{\beta_1})J^{2\beta_1} - (1 - \frac{1}{\beta_1})J^{\beta_1}\right) \\ &+ \left((2 + \frac{1}{\beta_2})J^{-2\beta_2} - (1 + \frac{1}{\beta_2})J^{-\beta_2}\right)\Bigg]\end{aligned} \tag{21}$$

Figure 12 schematically illustrates the effect of the parameters κ, β_1, and β_2, on the hydrostatic stress.

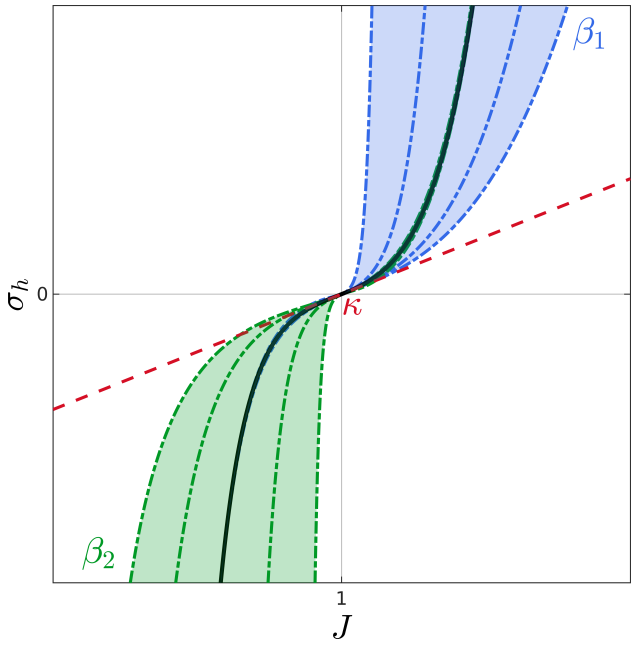

Figure 12: A schematic illustration of a typical σ_h curve illustrating the nature of the parameters κ, the bulk modulus setting the initial slope, β_1, setting the rate of strain stiffening in expansion, β_2, setting the rate of strain stiffening in shrinkage.

Figure 13 shows the effect of varying the bulk modulus κ.

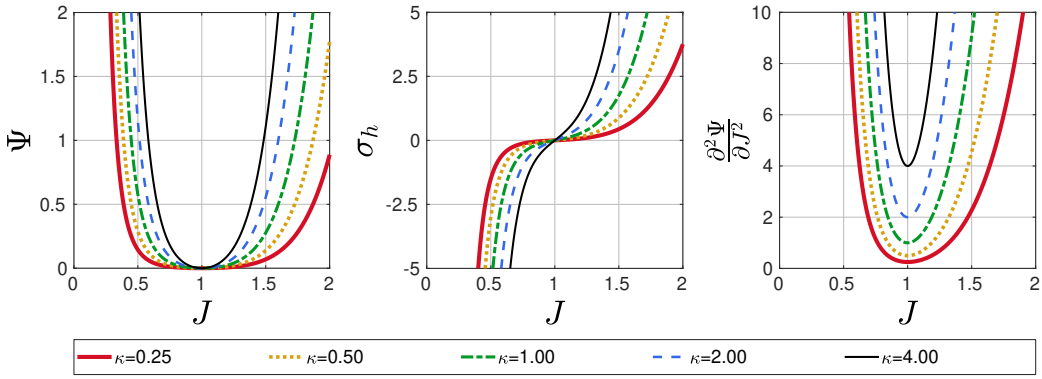

Figure 13: The effect of κ. The strain energy density (left), hydrostatic stress (middle), and tangent modulus (right) for formulation 1. Curves drawn for $\beta_1 = 4$, $\beta_2 = 2$, $\kappa = [0.25, 4]$.

Figure 14 and 15 illustrate the effect of varying β_1 and β_2 respectively, demonstrating near independent control of strain hardening for the expansion and shrinkage domains.

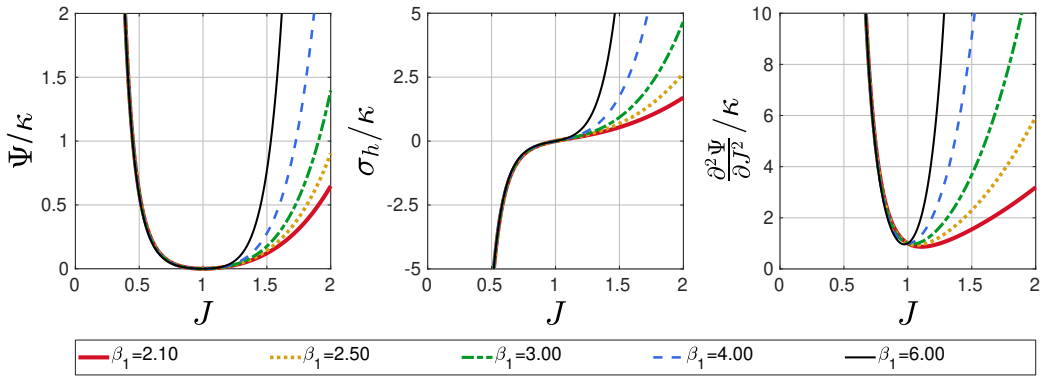

Figure 14: The effect of β_1. The normalized strain energy density (left), hydrostatic stress (middle), and tangent modulus (right) for formulation 1. Curves drawn for $\kappa = 1$, $\beta_2 = 2$, $\beta_1 = [2.1, 6]$.

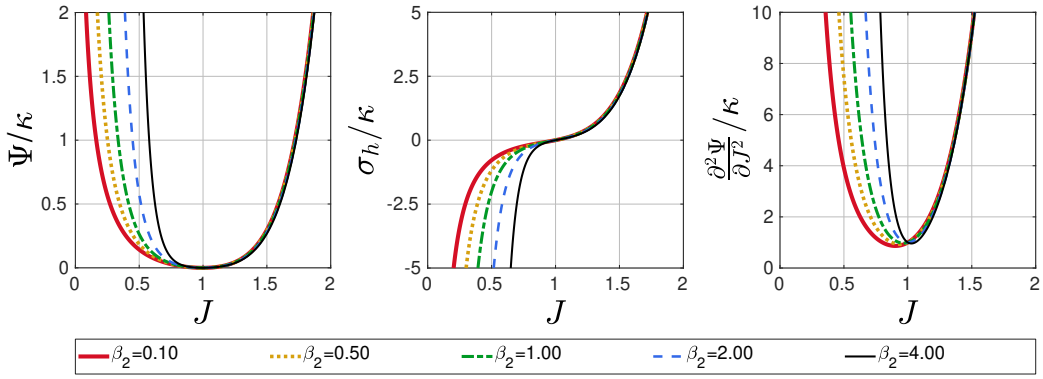

Figure 15: The effect of β_2. The normalized strain energy density (left), hydrostatic stress (middle), and tangent modulus (right) for formulation 1. Curves drawn for $\kappa = 1$, $\beta_1 = 4$, $\beta_2 = [0.1, 4]$.

Although near independent control is seen for both the magnitude and degree of strain stiffening of the responses for shrinkage and expansion, it is noted here that, similar to the Doll and Schweizerhof [10] formulation, the minimum stiffness is not guaranteed to be κ and may not be found at $J = 1$ (Note the shift in the minima for the tangent modulus in Figures 14 and 15). Formulation 2, discussed in the next section, avoids this behaviour.

In Appendix A two variations of the above formulation are briefly explored. In equation A.1 of Appendix A.1 a weighting factor was introduced with the aim of providing further control over the dominance of the expansion and shrinkage terms. However, this change results in a possible negative tangent modulus for particular parameter choices.

To address the fact that the minimum stiffness of formulation 1 only lies at $J = 1$ if $\beta_2 = \beta_1 + 2$, equation A.4 of Appendix A.2 describes a switch statement based decoupling of the expansion and shrinkage terms such that the expansion term is used if $J \geq 1$, and the shrinkage term if $J < 1$. Although this alternative form forces the minimum tangent modulus to occur at $J = 1$, and satisfies all constraints listed in Table 1, it presents with a non-smooth stiffness at $J = 1$, which may not be desirable.

4.2. Formulation 2

This section discusses a formulation which was inspired by the inverse sigmoid shape of the hydrostatic stress. A tangent function was chosen here since it presents with a rather elegant integral and derivative. The strain energy density for the proposed form is:

$$\Psi_{vol}(J) = -\kappa a^2 \ln\left(\cos\left(\frac{J-1}{a}\right)\right) \tag{22}$$

The derivative with J provides the hydrostatic stress:

$$\sigma_h(J) = \kappa a \tan\left(\frac{J-1}{a}\right) \tag{23}$$

The second derivative provides the tangent modulus:

$$\frac{\partial^2 \Psi_{vol}(J)}{\partial J^2} = \kappa \sec^2\left(\frac{J-1}{a}\right) \tag{24}$$

The parameter a is defined as:

$$a = \frac{2}{\pi}\begin{cases} (J_1 - 1) & J \geq 1 \\ (J_2 - 1) & J < 1 \end{cases} \tag{25}$$

This formulation features three material parameters, the bulk modulus κ and two volume ratio parameters defining "lock-up" stretches, J_1 (with $J_1 > 1$), and J_2 (with $0 \leq J_2 < 1$). Figure 16 contains a schematic illustration of the nature of these parameters in relation to the hydrostatic stress.

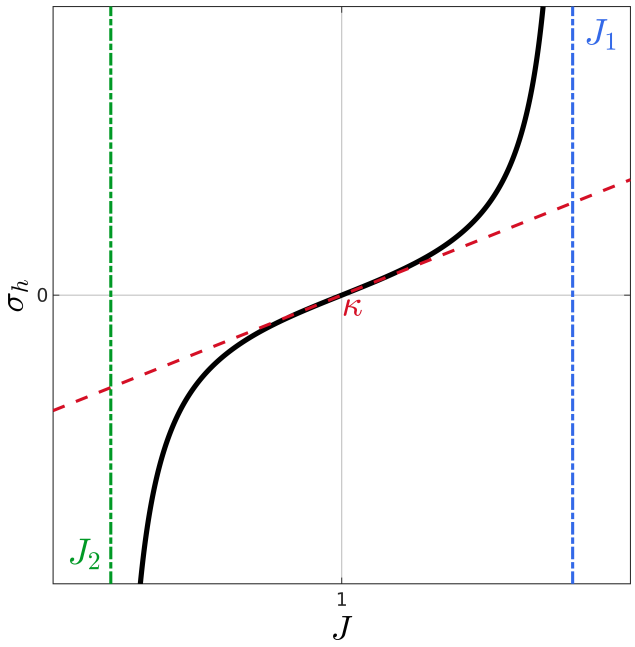

Figure 16: A schematic illustration of a typical σ_h curve illustrating the nature of the parameters κ, the bulk modulus setting the initial slope, J_1, setting the maximum volume ratio asymptote, and J_2, setting a minimum volume ratio asymptote.

Both J_1 and J_2 define a volume ratio at which an asymptote exists for strain energy, hydrostatic stress, and the tangent modulus. Numerical implementations therefore should feature the constraints:

$$\Psi_{vol}(J \geq J_1) = \Psi_{vol}(J \leq J_2) = \infty$$

$$\sigma_h(J \geq J_1) = -\sigma_h(J \leq J_2) = \infty \tag{26}$$

$$\frac{\partial^2 \Psi_{vol}(J \geq J_1)}{\partial J^2} = \frac{\partial^2 \Psi_{vol}(J \leq J_2)}{\partial J^2} = \infty$$

The bulk modulus κ sets the slope for the hydrostatic stress at $J = 1$. Beyond $J = 1$ the volume ratios J_1 and J_2 determine how rapidly stiffness is enhanced for the expansion and shrinkage domains. If a material exhibits a behaviour such that further volume change beyond a particular point is hindered, this can be modelled using an appropriate choice for these volume ratio asymptote levels. For many materials however $J_2 = 0$ is most appropriate as this is where this asymptote may naturally lie. Clearly if $J_2 = 0$ is kept fixed this formulation has only the two remaining parameters κ and J_1.

Both asymptote levels can be set at a level beyond the expected deformation levels or brought in closer to further enhance strain stiffening. Figure 17 illustrates the effect of varying the bulk modulus κ and demonstrates how it changes the slope at $J = 1$ for the hydrostatic stress.

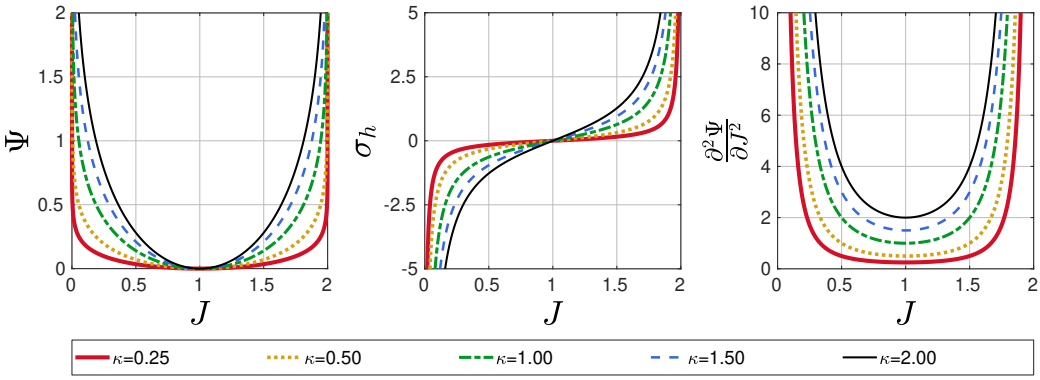

Figure 17: The effect of the bulk modulus. The normalized strain energy density (left), hydrostatic stress (middle), and tangent modulus (right) for formulation 2. Curves drawn for $J_2 = 0$, $J_1 = 2$ and $\kappa = [0.25, 2]$

Figure 18 presents the effect of varying J_1. The parameter J_1 is seen to shift the location of the asymptote in the expansion domain.

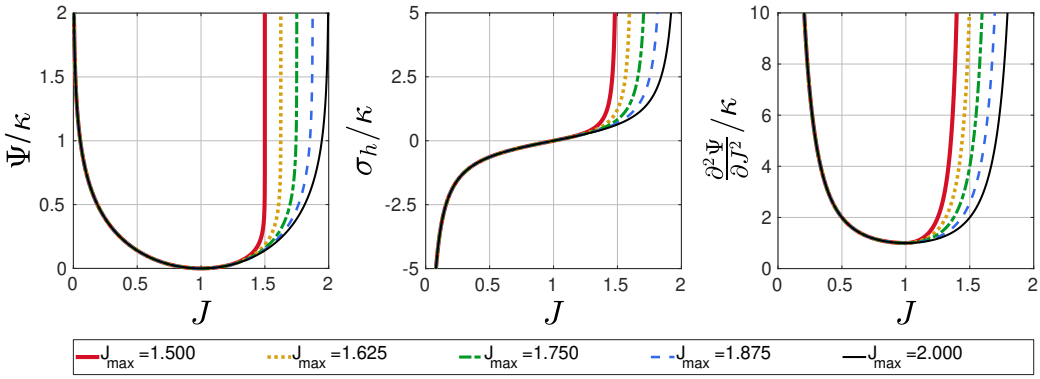

Figure 18: The effect of the J_1. The normalized strain energy density (left), hydrostatic stress (middle), and tangent modulus (right) for formulation 2. Curves drawn for $\kappa = 1$, $J_2 = 0$ and $J_1 = [1.5, 2]$

Figure 19 presents the effect of varying J_2. It is clear how J_2 enables one to alter the location of the asymptote in the shrinkage domain.

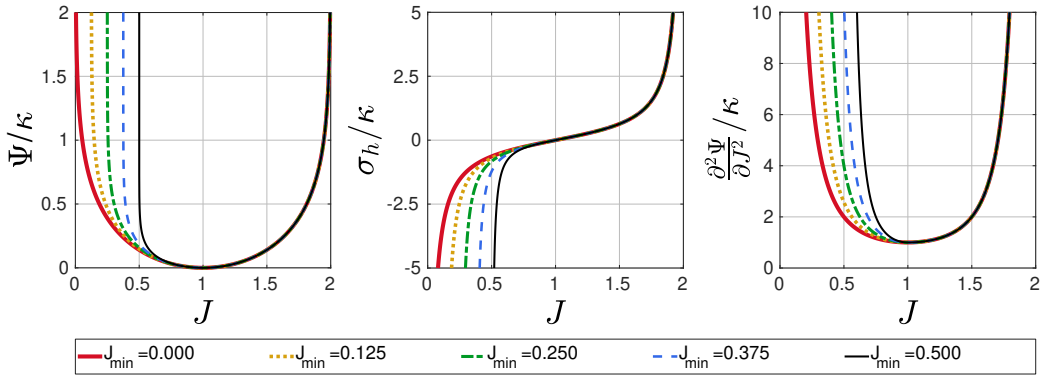

Figure 19: The effect of the J_2. The normalized strain energy density (left), hydrostatic stress (middle), and tangent modulus (right) for formulation 2. Curves drawn for $\kappa = 1$, $J_1 = 2$ and $J_2 = [0, 0.5]$

From Figures 17, 19, and 18 it is clear that, contrary to the other formulations, the minimum tangent modulus is guaranteed to occur at $J = 1$ and is equal to κ.

Furthermore, one may note that the following simultaneous symmetries exist:

$$\Psi_{vol}(J_s) = \Psi_{vol}(J_e), \quad \sigma_h(J_s) = -\sigma_h(J_e), \quad \frac{\partial^2 \Psi_{vol}(J_s)}{\partial J^2} = \frac{\partial^2 \Psi_{vol}(J_e)}{\partial J^2} \tag{27}$$

(where subscript s and e refer to shrinkage and expansion respectively), if

$$J_e = (J_s - 1)\frac{J_1 - 1}{J_2 - 1} + 1, \quad J_s = (J_e - 1)\frac{J_2 - 1}{J_1 - 1} + 1 \tag{28}$$

Therefore if simultaneous symmetry in terms of J and $1/J$ is desired one could use:

$$J_2 = \frac{1}{J_1} \tag{29}$$

Formulation 2 adheres to all criteria of Table 1, with the exception of criteria *VII* and *VIII*, due to the existence of the asymptote at J_1 in the expansion domain. Indeed it may be deemed unnatural to have the asymptote depart from $J = 0$ for the shrinkage domain, or to have an asymptote at all for the expansion domain. Appendix A.3 therefore presents a variation to formulation 2 which does not have these features, instead it employs a form similar to equation 7 but with natural asymptotic behaviour added at $J = 0$.

4.3. Formulation 3

Formulation 3, proposed below, is an extension of formulation 2, of Section 4.2, to capture non-monotonic strain stiffening, as observed in cellular materials, lattices, and foams [61, 5]. As illustrated in Figure 20, such materials exhibit three main phases during large volumetric compression [61]: I) an initial linear or moderately strain stiffening phase; II) a reduced stiffness/plateau region due to elastic buckling of the material microstructure; and III) a region of increased stiffness due to densification of the structure. Such non-monotonic stiffening behaviour with an elastic buckling plateau region is observed for elastometric foams, such as polyurethane foams (e.g. [13, 17]), and cork (e.g. [62, 5, 63, 47, 5]).

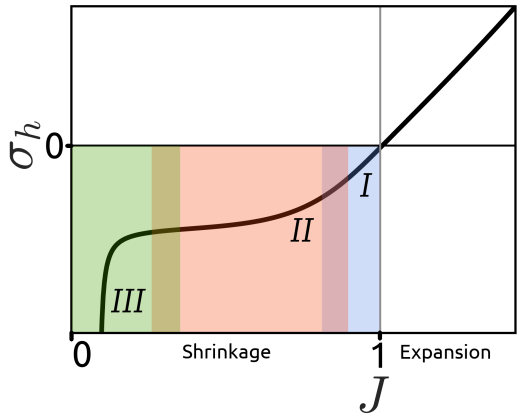

Figure 20: The typical response of a cellular solid to shrinkage and expansion. The shrinkage domain typically features several phases, e.g. an initial elastic domain (I), followed by a compaction domain (II), and a densification domain (III).

As seen in Section 4.2, Formulation 2 features the *tan* function creating a vertical sigmoid shape for the hydrostatic stress. In order to expand formulation 2 to allow for a reduced stiffness/plateau region, an additional horizontal sigmoid function is added; in this case a *tanh* function is used, with asymptotes parallel to the J axis. Conveniently these functions share conceptually similar integrals and derivatives. We propose the following strain energy density function:

$$\Psi_{vol}(J) = \kappa\left[-(1-q)a^2 \ln\left(\cos\left(\frac{J-1}{a}\right)\right) + qb^2 \ln\left(\cosh\left(\frac{J-1}{b}\right)\right)\right] \quad (30)$$

resulting in the following expression for hydrostatic stress:

$$\sigma_h(J) = \kappa\left[(1-q)a\tan\left(\frac{J-1}{a}\right) + qb\tanh\left(\frac{J-1}{b}\right)\right] \tag{31}$$

with the following expression for tangent modulus:

$$\frac{\partial^2\Psi_{vol}(J)}{\partial J^2} = \kappa\left[(1-q)\sec^2\left(\frac{J-1}{a}\right) + q\,\mathrm{sech}^2\left(\frac{J-1}{b}\right)\right] \tag{32}$$

The parameters a, b, and q are defined as:

$$a = \tfrac{2}{\pi}\begin{cases} (J_1-1) & J \geq 1 \\ \\ (J_2-1) & J < 1 \end{cases} \qquad b = \tfrac{1}{\kappa}\begin{cases} s_1 & J \geq 1 \\ \\ s_2 & J < 1 \end{cases} \qquad q = \begin{cases} q_1 & J \geq 1 \\ \\ q_2 & J < 1 \end{cases} \tag{33}$$

In all cases independent values can be specified for shrinkage ($J < 1$) and expansion ($J > 1$). The parameter a is the same as for formulation 2 where J_2 and J_1 set the volume ratios for the two vertical asymptotes. Parameters s_2 and s_1 set the hydrostatic stress asymptotes of the horizontal sigmoid function ($tanh$) in expansion and shrinkage, respectively. The parameters q_1 and q_2 set the relative contributions of the monotonic strain stiffening behaviour of the tan component and the hydrostatic stress plateau behaviour of the $tanh$ component. If $q_i = 0$ formulation 2 is recovered, with monotonic strain stiffening. Conversely, if $q_i = 1$ a plateau in hydrostatic stress is obtained, but this is not followed by a high stiffness densification region. Figure 21 is a schematic illustration to highlight the effect of the material parameters on the hydrostatic stress. The six physically based parameters can be used to precisely specify the three phases of volumetric deformation described above.

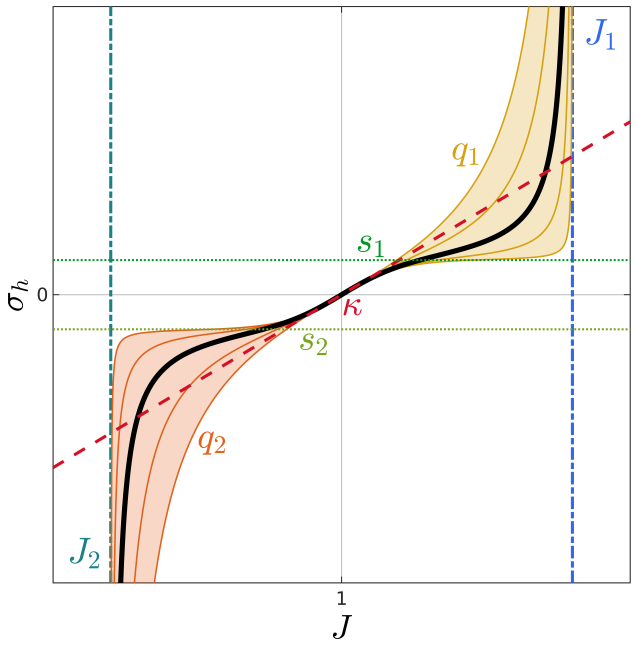

Figure 21: A schematic illustration of a typical σ_h curve illustrating the nature of the parameters κ, the bulk modulus setting the initial slope, J_1, setting the maximum volume ratio asymptote, and J_2, setting a minimum volume ratio asymptote, s_1, setting the softening stress in expansion, q_1 setting the dominance of the softening in expansion, s_2, setting the softening stress in shrinkage, and q_2 setting the dominance of the softening in shrinkage.

We next provide a parametric investigation of the effect of varying the parameters s_1, s_2, q_1, and q_2. The effect of κ, J_1 and J_2 is equivalent to that of formulation 2 (see Figure 17, 19, and 18 respectively) and therefore not repeated graphically here. Figure 22 shows the effect of varying s_1. This parameter sets the plateau stress level for expansion for the horizontal sigmoid function.

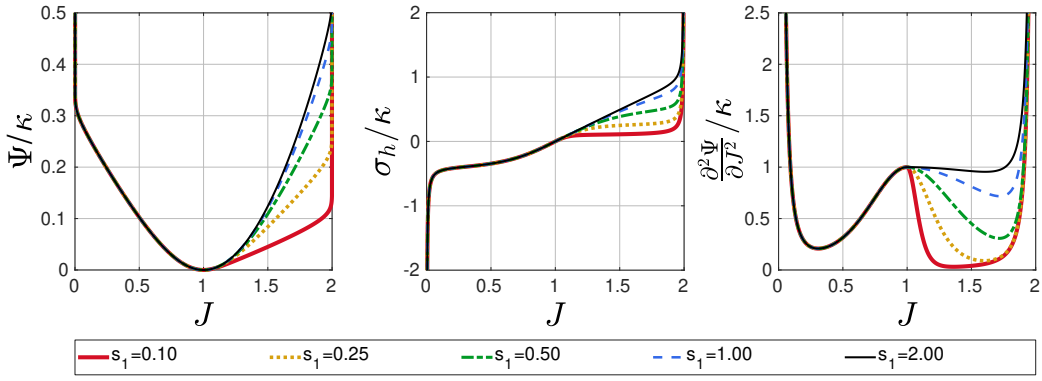

Figure 22: The effect of the s_1. The normalized strain energy density (left), hydrostatic stress (middle), and tangent modulus (right) for formulation 3. Curves drawn for $\kappa = 1$, $J_1 = 2$, $J_2 = 0$, $q_1 = 0.98$, $q_2 = 0.98$, $s_1 = [0.1, 2]$, $s_2 = 0.4$

Figure 23 shows the effect of varying s_2. This parameter sets the plateau stress level for shrinkage for the horizontal sigmoid function (note that although the hydrostatic stress is negative during shrinkage, s_2 is here defined as a positive number).

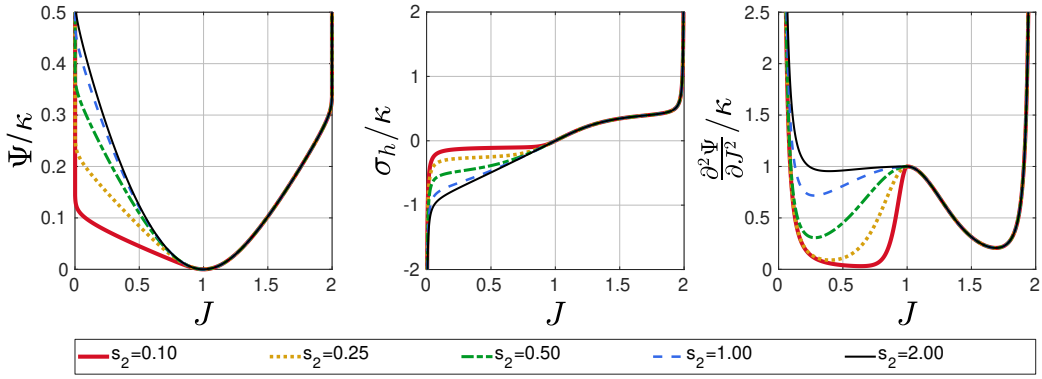

Figure 23: The effect of the s_2. The normalized strain energy density (left), hydrostatic stress (middle), and tangent modulus (right) for formulation 3. Curves drawn for $\kappa = 1$, $J_1 = 2$, $J_2 = 0$, $q_1 = 0.98$, $q_2 = 0.98$, $s_1 = 0.4$, $s_2 = [0.1, 2]$

Figure 24 presents the effect of varying q_1, which controls the dominance of the stiffness reduction/plateau behaviour in the expansion domain.

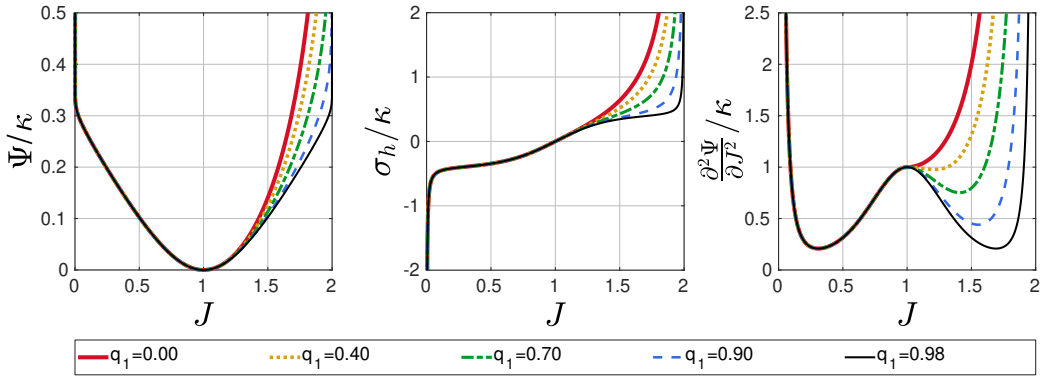

Figure 24: The effect of the q_1. The normalized strain energy density (left), hydrostatic stress (middle), and tangent modulus (right) for formulation 3. Curves drawn for $\kappa = 1$, $J_1 = 2$, $J_2 = 0$, $q_1 = [0, 0.98]$, $q_2 = 0.98$, $s_1 = 0.4$, $s_2 = 0.4$

Figure 25 presents the effect of varying q_2, which controls the dominance of the stiffness reduction/plateau behaviour in the shrinkage domain.

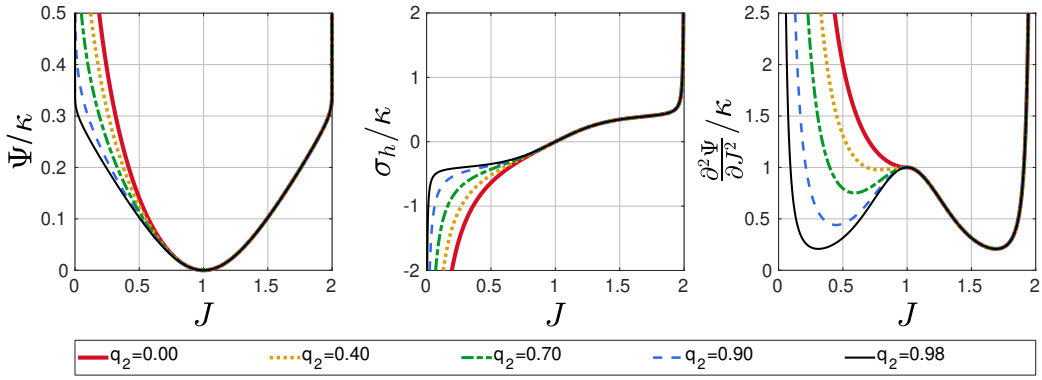

Figure 25: The effect of the q_2. The normalized strain energy density (left), hydrostatic stress (middle), and tangent modulus (right) for formulation 3. Curves drawn for $\kappa = 1$, $J_1 = 2$, $J_2 = 0$, $q_1 = 0.98$, $q_2 = [0, 0.98]$, $s_1 = 0.4$, $s_2 = 0.4$

4.4. Fitting to experimental data

To illustrate the ability of our new formulation 1-3 to capture experimental hydrostatic compression data, Figure 26 presents fits to data for neoprene rubber foam [45] (1^{st} column), flexible open-cell polyurethane cushioning foam [17] (2^{nd} column), natural cork [46] (3^{rd} column), and rigid closed-cell polyurethane foam [47] (4^{th} column). For all fits the bulk-modulus κ was

kept fixed and was instead derived from the slope calculated for the small strain domain (up to 4% shrinkage).

As is evident from Figure 26, an increasing amounts of stiffness reduction/plateau behaviour is observed in the experimental data (from left to right). In the case of the neoprene and open-cell foam the data represents fully elastic recoverable loading associated with elastic buckling of the microstructure (rather than unrecoverable plastic buckling). Formulation 1 cannot accurately capture the non-linear monotonic strain stiffening behavior of noeprene rubber foam; the high stiffness behaviour at high volumetric strains is accurately predicted, but the stiffness at low volumetric strains is under predicted. In contrast, formulation 2 accurately predicts the neoprene rubber foam behavour for the full range of experimental data. However, the inflection point observed for open-cell polyurethane cushioning foam and natural cork, and the plateau behaviour for closed-cell polyurethane foam are not captured. Formulation 3 is shown to accurately predict the reported experimental data for all four materials.

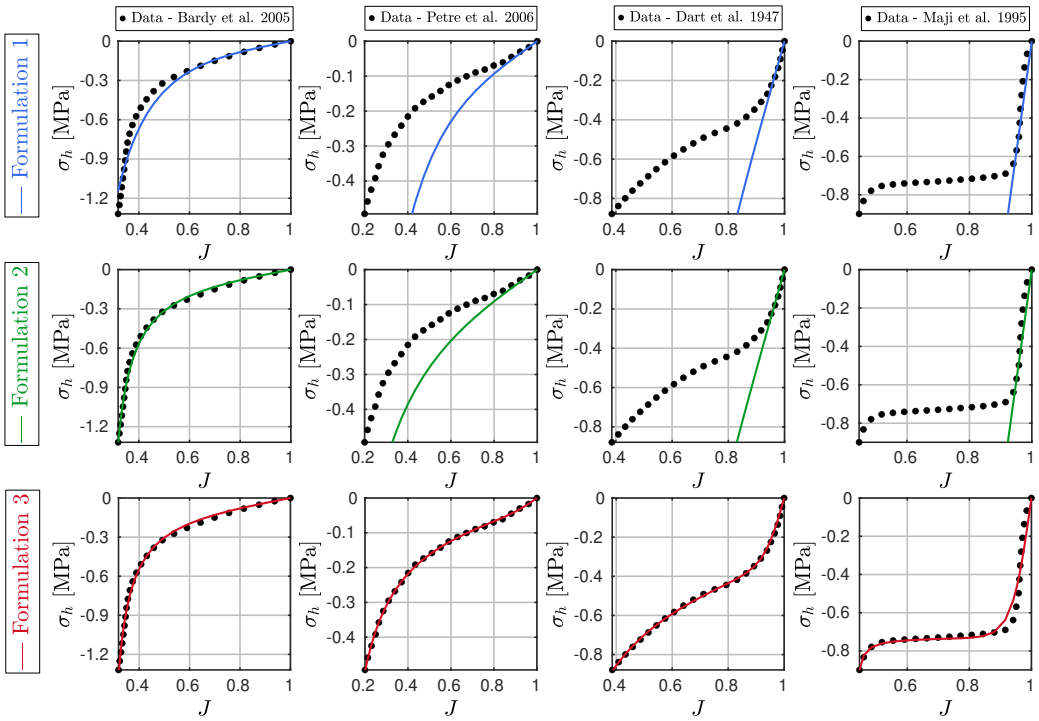

Figure 26: Fitting of formulation 1 (top row), formulation 2 (middle row), and formulation 3 (bottom row) to experimental hydrostatic compression data. From the left to the right the data was obtained from Bardy et al. [45], Petre et al. [17], Dart et al. [46], and , Maji et al. [47].

5. Discussion

Much attention has been given to the development of deviatoric strain energy density functions due to the traditional focus, of hyperelastic modelling, on nearly-incompressible rubber materials (e.g. [33, 35, 34]), and assumed incompressible soft tissue [6]. Comparatively few strain energy density functions have been proposed for large volumetric deformations (e.g. [9, 7, 8, 10, 51]). We demonstrate here that well-established and commonly used volumetric strain energy formulations are either not valid for large volumetric deformations, as they (i) do not adhere to criteria *I*-*IX* of Table 1, or (ii) do not offer sufficient control, for either the shrinkage or the expansion domain, for fitting of monotonic or non-monotonic strain stiffening behaviour (criteria *X* of Table 1). Following a summary and critical analysis of common formulations, and the pitfalls they exhibit, we propose three

novel formulations which uniquely: 1) are valid for large volumetric deformations, 2) offer separate control of the volumetric strain stiffening behaviour during shrinkage (volume reduction) and expansion (volume increase), and 3) in the case of formulation 3, offer the ability to capture non-monotonic volumetric stiffening. The presented formulations offer superior flexibility for experimental fitting of the large volumetric strain behaviour of hyperelastic materials, and are demonstrated to adhere to all physical constraints and criteria listed in Table 1.

- Formulation 1 (Section 4.1) exhibits control of the magnitude and degree of strain stiffening in shrinkage and expansion domains which is not strongly coupled. This presents an incremental improvement of on the model of Doll and Schweizerhof [10], in which the degree of strain stiffening in shrinkage and expansion is strongly coupled. One property of formulation 1 however is that the minimum of the tangent modulus may not occur at $J = 1$, and is therefore lower than κ, for a particular choice of parameters. Although this is a property shared with many other formulations, and this does not render the formulation invalid by any means, it may be deemed undesirable or unrealistic given particular experimental data.

- Formulation 2 (Section 4.2) was developed to exhibit many of the properties of formulation 1 but also guarantees that the minimum stiffness is found at $J = 1$. This model is formulated using logarithmic and trigonometric functions, and features a bulk modulus κ to set the initial slope and two controllable asymptotes, one at the volume ratio J_1 for expansion, and one at the volume ratio J_2 for shrinkage. For shrinkage J_2 can be set at 0 to enable, for instance, infinite strain energy at $J = 0$, as is common. However, it is possible to bring J_2 closer to 1 to enable more rapid stiffening during volume reduction. Similarly J_1 is the volume ratio at which an asymptote exists for volume expansion. Control of strain stiffening in shrinkage and expansion domains is fully decoupled, i.e. changes in one domain do not influence the other. In terms of achieving symmetry, formulation 2 also enables, through an appropriate choice of parameters, simultaneous symmetry in terms of $\Psi_{vol}(J) = \Psi_{vol}(\frac{1}{J})$, $p(J) = -p(\frac{1}{J})$, and $\partial^2\Psi_{vol}(J)/\partial J^2 = \partial^2\Psi_{vol}(\frac{1}{J})/\partial J^2$, i.e. the strain energy density, hydrostatic stress and tangent modulus for a given percentage volume

increase or decrease can be made to be equivalent. Furthermore, formulation 2 ensures that, even for deviations from symmetry, the minimum tangent modulus always occurs at $J = 1$ and is equal to κ. Appendix A.3 provides a variation to formulation 2 whereby the asymptote parameters are avoided.

- Formulation 3 (Section 4.3) extends formulation 2, of Section 4.2, to capture the non-monotonic stiffening reported for cellular materials, lattices, and foams [61, 5]. A horizontal sigmoid function is superimposed on formulation 2 creating softening behaviour. The parameters s_1 and s_2 define hydrostatic stress asymptotes on the horizontal sigmoid function for the expansion and shrinkage domain respectively. Furthermore parameters q_1 or q_2 define the dominance of these potential softening plateaus. Similar to formulation 2, formulation 3 offers independent control of the behaviour for the expansion and shrinkage domains.

Formulation 3 is shown to provide accurate predictions of the non-linear pressure volumetric relationship under hydrostatic compression for four materials, namely: neoprene rubber foam [45], flexible open-cell polyurethane cushioning foam [17], natural cork [46], and rigid closed-cell polyurethane foam [47]. As discussed above, the ability to accurately model non-monotonic volumetric shrinkage and expansion will be important for the simulation and design of next-generation lattice materials, including ultraporous sponges [26] graphene foams aerogels (e.g [27, 28, 29, 30]) in which elastic recovery from compressive strains of 90% have been reported [31]. Graphene aerogels can also be 3D printed [64] allowing for the creation of highly elastic, deformable, and complex lattices structures. Formulation 3 can also be used to simulate non-monotonic volumetric stiffening of compressible biological materials, such as arteries [65], and the myocardium [66]. Formulation 3 can also be extended to account for plastic buckling in the plateau region (as observed for polypropylene foams [67], metallic foams [68], and trabecular bone [69, 70].

Figure 27 presents two examples of highly elastic lattice structures which can be 3D printed in rubber-like polymeric materials. The lattices are subjected to hydrostatic deformations. The structure and visualizations are based on dedicated finite element (FEBio 2.9.1 [57]) models (the lattice is meshed using hexahedral elements, solid material is represented as Neo-Hookean, i.e. $\psi = \frac{c}{4}\big(\operatorname{tr}(\tilde{\mathbf{C}})-3\big)+\frac{\kappa}{2}\ln(J)^2$, with $c = 1$ MPa, and $\kappa = 50$ MPa.

A related demo has been made available open source as part of GIBBON [52]: `DEMO_febio_0054_lattice_hydrostatic_01.m`). The top row in figure 27 is for the regular octet-truss lattice structure, which demonstrates fairly linear behaviour in expansion and non-linear plateauing and densification during shrinkage due to elastic buckling of struts. The bottom row is for an octet-truss lattice with initially curved features. Such features are straightened during expansion creating a source of stiffness enhancement. During shrinkage however the initially curved features immediately and gradually continue to bend, resulting in the absence of the more sudden initiation of bending seen in the structure of the top row.

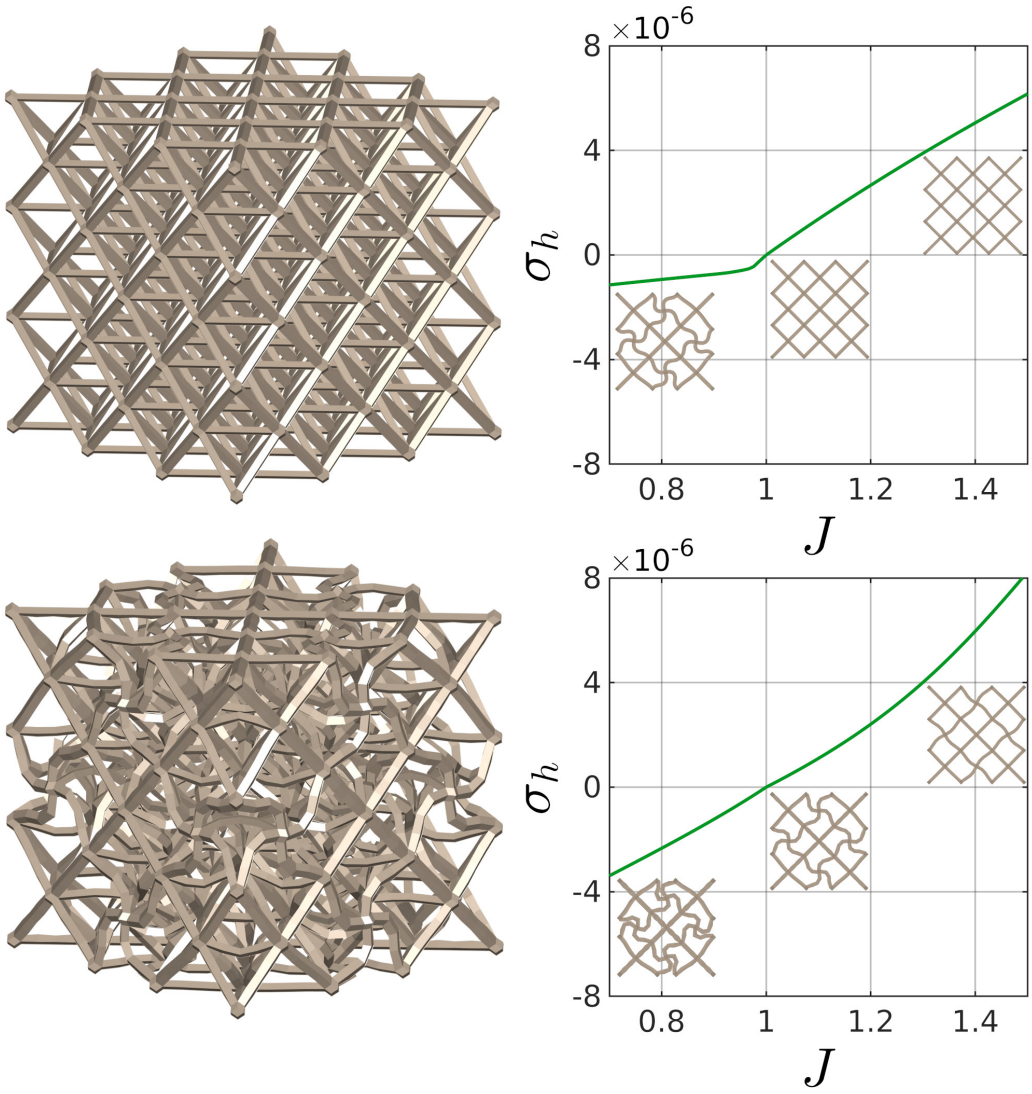

Figure 27: Two types of octet truss lattice structures subjected to hydrostatic loading. Graphs on the right show hydrostatic stress (σ_h) as a function of the volume ratio (J). The initial configuration for each lattice is shown in 3D on the left. 2D views of the initial and loaded configurations are also visualized schematically within the graphs on the right. The top row is for a regular octet-truss lattice while the bottom row is for an octet-truss lattice with initially curved features.

Future work will include the use of the presented formulations for modelling of highly compliant 3D printed polymer lattice structures with tailorable strain stiffening and densification behaviour. Such materials are use-

ful for the design of custom biomechanical support structures e.g. at the interface between tissue and prosthetic or orthotic devices.

6. Acknowledgements

This project was funded by a European Union Horizon 2020 Research and Innovation Program, under grant agreement No. 777072.

References

[1] T. A. Schaedler, W. B. Carter, Architected Cellular Materials, Annual Review of Materials Research 46 (2016) 187–210.

[2] Fleck N. A., Deshpande V. S., Ashby M. F., Micro-architectured materials: past, present and future, Proceedings of the Royal Society A: Mathematical, Physical and Engineering Sciences 466 (2010) 2495–2516.

[3] J. W. C. Dunlop, P. Fratzl, Multilevel architectures in natural materials, Scripta Materialia 68 (2013) 8–12.

[4] Mihai L. Angela, Alayyash Khulud, Goriely Alain, Paws, pads and plants: the enhanced elasticity of cell-filled load-bearing structures, Proceedings of the Royal Society A: Mathematical, Physical and Engineering Sciences 471 (2015) 20150107.

[5] L. J. Gibson, K. E. Easterling, M. F. Ashby, The structure and mechanics of cork, Proceedings of the Royal Society of London. A. Mathematical and Physical Sciences 377 (1981) 99–117.

[6] G. Chagnon, M. Rebouah, D. Favier, Hyperelastic energy densities for soft biological tissues: A review, Journal of Elasticity 120 (2015) 129–160.

[7] J. E. Bischoff, E. M. Arruda, K. Grosh, A New Constitutive Model for the Compressibility of Elastomers at Finite Deformations, Rubber Chemistry and Technology 74 (2001) 541–559.

[8] B. Storåkers, On material representation and constitutive branching in finite compressible elasticity, Journal of the Mechanics and Physics of Solids 34 (1986) 125–145.

[9] R. W. Ogden, Large Deformation Isotropic Elasticity: On the Correlation of Theory and Experiment for Compressible Rubberlike Solids, Proceedings of the Royal Society A: Mathematical, Physical and Engineering Sciences 328 (1972) 567–583.

[10] S. Doll, K. Schweizerhof, On the Development of Volumetric Strain Energy Functions, Journal of Applied Mechanics 67 (2000) 17–21.

[11] N. J. Mills, C. Fitzgerald, A. Gilchrist, R. Verdejo, Polymer foams for personal protection: cushions, shoes and helmets, Composites Science and Technology 63 (2003) 2389–2400.

[12] L. Savonnet, X. Wang, S. Duprey, Finite element models of the thigh-buttock complex for assessing static sitting discomfort and pressure sore risk: a literature review, Computer Methods in Biomechanics and Biomedical Engineering 21 (2018) 379–388.

[13] D. Y. Kim, J. H. Bang, C. A. Lee, H. Y. Kim, K. Y. Choi, B. G. Lim, Numerical evaluation of time-dependent sagging for low density polyurethane foams to apply the long-term driving comfort on the seat cushion design, International Journal of Industrial Ergonomics 64 (2018) 178–187.

[14] C. Briody, B. Duignan, S. Jerrams, J. Tiernan, The implementation of a visco-hyperelastic numerical material model for simulating the behaviour of polymer foam materials, Computational Materials Science 64 (2012) 47–51.

[15] L. P. Cohen, A. Gefen, Deep tissue loads in the seated buttocks on an off-loading wheelchair cushion versus air-cell-based and foam cushions: finite element studies, International Wound Journal 14 (2017) 1327–1334.

[16] E. Palta, H. Fang, D. C. Weggel, Finite element analysis of the Advanced Combat Helmet under various ballistic impacts, International Journal of Impact Engineering 112 (2018) 125–143.

[17] M. T. Petre, A. Erdemir, P. R. Cavanagh, Determination of elastomeric foam parameters for simulations of complex loading, Computer Methods in Biomechanics and Biomedical Engineering 9 (2006) 231–242.

[18] R. L. Actis, L. B. Ventura, D. J. Lott, K. E. Smith, P. K. Commean, M. K. Hastings, M. J. Mueller, Multi-plug insole design to reduce peak plantar pressure on the diabetic foot during walking, Medical & Biological Engineering & Computing 46 (2008) 363–371.

[19] A. Ghassemi, A. R. Mossayebi, N. Jamshidi, R. Naemi, M. T. Karimi, Manufacturing and finite element assessment of a novel pressure reduc-

ing insole for Diabetic Neuropathic patients, Australasian Physical & Engineering Sciences in Medicine 38 (2015) 63–70.

[20] B. C. M. Murray, X. An, S. S. Robinson, I. M. v. Meerbeek, K. W. O'Brien, H. Zhao, R. F. Shepherd, Poroelastic Foams for Simple Fabrication of Complex Soft Robots, Advanced Materials 27 (2015) 6334–6340.

[21] N. G. Cheng, A. Gopinath, L. Wang, K. Iagnemma, A. E. Hosoi, Thermally Tunable, Self-Healing Composites for Soft Robotic Applications, Macromolecular Materials and Engineering 299 (2014) 1279–1284.

[22] C. Schlagenhauf, D. Bauer, K. Chang, J. P. King, D. Moro, S. Coros, N. Pollard, Control of Tendon-Driven Soft Foam Robot Hands, in: 2018 IEEE-RAS 18th International Conference on Humanoid Robots (Humanoids), pp. 1–7.

[23] L. Somm, D. Hahn, N. Kumar, S. Coros, Expanding Foam as the Material for Fabrication, Prototyping and Experimental Assessment of Low-Cost Soft Robots With Embedded Sensing, IEEE Robotics and Automation Letters 4 (2019) 761–768.

[24] L. R. Meza, S. Das, J. R. Greer, Strong, lightweight, and recoverable three-dimensional ceramic nanolattices, Science 345 (2014) 1322–1326.

[25] M. R. Islam, G. Tudryn, R. Bucinell, L. Schadler, R. C. Picu, Stochastic continuum model for mycelium-based bio-foam, Materials & Design 160 (2018) 549–556.

[26] M. Mader, V. Jrme, R. Freitag, S. Agarwal, A. Greiner, Ultraporous, Compressible, Wettable Polylactide/Polycaprolactone Sponges for Tissue Engineering, Biomacromolecules 19 (2018) 1663–1673.

[27] D. Pan, C. Wang, X. Wang, Graphene Foam: Hole-Flake Network for Uniaxial Supercompression and Recovery Behavior, ACS Nano 12 (2018) 11491–11502.

[28] J. Shang, Q.-S. Yang, X. Liu, C. Wang, Compressive deformation mechanism of honeycomb-like graphene aerogels, Carbon 134 (2018) 398–410.

[29] Y. Wu, N. Yi, L. Huang, T. Zhang, S. Fang, H. Chang, N. Li, J. Oh, J. A. Lee, M. Kozlov, A. C. Chipara, H. Terrones, P. Xiao, G. Long, Y. Huang, F. Zhang, L. Zhang, X. Lepr, C. Haines, M. D. Lima, N. P. Lopez, L. P. Rajukumar, A. L. Elias, S. Feng, S. J. Kim, N. T. Narayanan, P. M. Ajayan, M. Terrones, A. Aliev, P. Chu, Z. Zhang, R. H. Baughman, Y. Chen, Three-dimensionally bonded spongy graphene material with super compressive elasticity and near-zero Poissons ratio, Nature Communications 6 (2015) 6141.

[30] S. Chandrasekaran, P. G. Campbell, T. F. Baumann, M. A. Worsley, Carbon aerogel evolution: Allotrope, graphene-inspired, and 3d-printed aerogels, Journal of Materials Research 32 (2017) 4166–4185.

[31] H. Hu, Z. Zhao, W. Wan, Y. Gogotsi, J. Qiu, Ultralight and Highly Compressible Graphene Aerogels, Advanced Materials 25 (2013) 2219–2223.

[32] V. Tutwiler, R. I. Litvinov, A. P. Lozhkin, A. D. Peshkova, T. Lebedeva, F. I. Ataullakhanov, K. L. Spiller, D. B. Cines, J. W. Weisel, Kinetics and mechanics of clot contraction are governed by the molecular and cellular composition of the blood, Blood 127 (2016) 149–159.

[33] R. S. Rivlin, D. W. Saunders, Large Elastic Deformations of Isotropic Materials. VII. Experiments on the Deformation of Rubber, Philosophical Transactions of the Royal Society A: Mathematical, Physical and Engineering Sciences 243 (1951) 251–288.

[34] L. R. G. Treloar, H. G. Hopkins, R. S. Rivlin, J. M. Ball, The Mechanics of Rubber Elasticity, Proceedings of the Royal Society A: Mathematical, Physical and Engineering Sciences 351 (1976) 301–330.

[35] R. Ogden, Non-linear elastic deformations, Dover Publications Inc., 1984.

[36] M. C. Boyce, E. M. Arruda, Constitutive Models of Rubber Elasticity: A Review, Rubber Chemistry and Technology 73 (2000) 504–523.

[37] J. C. Simo, R. L. Taylor, Penalty function formulations for incompressible nonlinear elastostatics, Computer Methods in Applied Mechanics and Engineering 35 (1982) 107–118.

[38] J. A. Weiss, B. N. Maker, S. Govindjee, Finite element implementation of incompressible, transversely isotropic hyperelasticity, Computer Methods in Applied Mechanics and Engineering 135 (1996) 107–128.

[39] R. Hill, Aspects of Invariance in Solid Mechanics, in: C.-S. Yih (Ed.), Advances in Applied Mechanics, volume 18, Elsevier, 1979, pp. 1–75.

[40] P. J. Blatz, W. L. Ko, Application of Finite Elastic Theory to the Deformation of Rubbery Materials, Transactions of the Society of Rheology 6 (1962) 223–252.

[41] F. A. O. Fernandes, R. T. Jardin, A. B. Pereira, R. J. Alves de Sousa, Comparing the mechanical performance of synthetic and natural cellular materials, Materials & Design 82 (2015) 335–341.

[42] Z. Liu, M. G. Scanlon, Modelling Indentation of Bread Crumb by Finite Element Analysis, Biosystems Engineering 85 (2003) 477–484.

[43] M. Ju, S. Mezghani, H. Jmal, R. Dupuis, E. Aubry, Parameter Estimation of a Hyperelastic Constitutive Model for the Description of Polyurethane Foam in Large Deformation, Cellular Polymers 32 (2013) 21–40.

[44] B. Fazekas, T. J. Goda, Determination of the hyper-viscoelastic model parameters of open-cell polymer foams and rubber-like materials with high accuracy, Materials & Design 156 (2018) 596–608.

[45] E. Bardy, J. Mollendorf, D. Pendergast, Thermal conductivity and compressive strain of foam neoprene insulation under hydrostatic pressure, Journal of Physics D: Applied Physics 38 (2005) 3832–3840.

[46] S. L. Dart, H. A. Robinson, E. Guth, Elastic Properties of Cork: III. Hydrostatic and Ordinary LoadCompression Curves for Cork, Journal of Applied Physics 18 (1947) 474–478.

[47] A. Maji, H. Schreyer, S. Donald, Q. Zuo, D. Satpathi, Mechanical Properties of Polyurethane-Foam Impact Limiters, Journal of Engineering Mechanics 121 (1995) 528–540.

[48] G. Holzapfel, Nonlinear solid mechanics: A continuum approach for engineering, John Wiley & Sons Ltd., 2000.

[49] C. O. Horgan, J. G. Murphy, On the volumetric part of strain-energy functions used in the constitutive modeling of slightly compressible solid rubbers, International Journal of Solids and Structures 46 (2009) 3078–3085.

[50] W. Ehlers, G. Eipper, The simple tension problem at large volumetric strains computed from finite hyperelastic material laws, Acta Mechanica 130 (1998) 17–27.

[51] G. Montella, S. Govindjee, P. Neff, The Exponentiated Hencky Strain Energy in Modeling Tire Derived Material for Moderately Large Deformations, Journal of Engineering Materials and Technology 138 (2016).

[52] K. M. Moerman, GIBBON: The Geometry and Image-Based Bioengineering add-On, The Journal of Open Source Software 3 (2018) 506.

[53] K. Moerman, A. J. Nederveen, C. K. Simms, Image Based Model Construction , Boundary Condition Specification and Inverse Fea Control : a Basic Matlab Toolkit for Febio, Proceedings of the 11th International Symposium, Computer Methods in Biomechanics and Biomedical Engineering (2013) 7–8.

[54] H. Hencky, The elastic behavior of vulcanized rubber, Rubber Chemistry and Technology 6 (1933) 217–224.

[55] T. Sussman, K.-J. Bathe, A finite element formulation for nonlinear incompressible elastic and inelastic analysis, Computers & Structures 26 (1987) 357–409.

[56] J. C. Simo, A framework for finite strain elastoplasticity based on maximum plastic dissipation and the multiplicative decomposition: Part i. continuum formulation, Computer Methods in Applied Mechanics and Engineering 66 (1988) 199–219.

[57] S. A. Maas, B. J. Ellis, G. A. Ateshian, J. A. Weiss, FEBio: Finite elements for biomechanics, Journal of Biomechanical Engineering 134 (2012) 011005–011005.

[58] E. M. Arruda, M. C. Boyce, A three-dimensional constitutive model for the large stretch behavior of rubber elastic materials, Journal of the Mechanics and Physics of Solids 41 (1993) 389–412.

[59] H. F. Enderle, H. G. Kilian, T. Vilgis, Irreversible deformation of macromolecular networks, Colloid and Polymer Science 262 (1984) 696–704.

[60] H. F. Enderle, H. G. Kilian, General deformation modes of a van der Waals network, in: Permanent and Transient Networks, Progress in Colloid & Polymer Science, Steinkopff, 1987, pp. 55–61.

[61] L. J. Gibson, Biomechanics of cellular solids, Journal of Biomechanics 38 (2005) 377–399.

[62] M. Fortes, J. Fernandes, I. Serralheiro, M. Rosa, Experimental Determination of Hydrostatic Compression versus Volume Change Curves for Cellular Solids, Journal of Testing and Evaluation 17 (1989) 67.

[63] L. Le Barbenchon, J. Girardot, J.-B. Kopp, P. Viot, Multi-scale foam : 3d structure/compressive behaviour relationship of agglomerated cork, Materialia 5 (2019) 100219.

[64] Q. Zhang, F. Zhang, S. P. Medarametla, H. Li, C. Zhou, D. Lin, 3d Printing of Graphene Aerogels, Small 12 (2016) 1702–1708.

[65] D. R. Nolan, J. P. McGarry, On the Compressibility of Arterial Tissue, Annals of Biomedical Engineering 44 (2016) 993–1007.

[66] E. McEvoy, G. A. Holzapfel, P. McGarry, Compressibility and Anisotropy of the Ventricular Myocardium: Experimental Analysis and Microstructural Modeling, Journal of Biomechanical Engineering 140 (2018) 081004–081004–10.

[67] P. Viot, Hydrostatic compression on polypropylene foam, International Journal of Impact Engineering 36 (2009) 975–989.

[68] V. S. Deshpande, N. A. Fleck, Multi-axial yield behaviour of polymer foams, Acta Materialia 49 (2001) 1859–1866.

[69] N. Kelly, J. P. McGarry, Experimental and numerical characterisation of the elasto-plastic properties of bovine trabecular bone and a trabecular bone analogue, Journal of the Mechanical Behavior of Biomedical Materials 9 (2012) 184–197.

[70] N. Kelly, N. M. Harrison, P. McDonnell, J. P. McGarry, An experimental and computational investigation of the post-yield behaviour of trabecular bone during vertebral device subsidence, Biomechanics and Modeling in Mechanobiology 12 (2013) 685–703.

Appendix A. Alternative formulations

Appendix A.1. Formulation 1 with a weighting factor

In this variation of formulation 1 of section 4.1 a weighting factor $q \in [0, 1]$ is introduced with the aim of scaling the contributions for expansion and shrinkage. The strain energy density for this variation is:

$$\Psi_{vol}(J) = \frac{\kappa}{2}\left(\frac{q}{{\beta_1}^2}(J^{\beta_1} - 1)^2 + \frac{1-q}{{\beta_2}^2}(J^{-\beta_2} - 1)^2\right) \tag{A.1}$$

Leading to the following expression for the hydrostatic stress:

$$\sigma_h(J) = \frac{\kappa}{J}\left(\frac{q}{\beta_1}(J^{2\beta_1} - J^{\beta_1}) - \frac{1-q}{\beta_2}(J^{-2\beta_2} - J^{-\beta_2})\right) \tag{A.2}$$

and the tangent modulus:

$$\begin{aligned}\frac{\partial^2 \Psi_{vol}(J)}{\partial J^2} = \frac{\kappa}{J^2}\Bigg[&\frac{q}{\beta_1}\left((2\beta_1 - 1)J^{2\beta_1} - (\beta_1 - 1)J^{\beta_1}\right) \\ &+ \frac{1-q}{\beta_2}\left((2\beta_2 + 1)J^{-2\beta_2} - (\beta_2 + 1)J^{-\beta_2}\right)\Bigg]\end{aligned} \tag{A.3}$$

It is noted that if $q = 1$ and $\beta_1 = 1$ this formulation reduces to the familiar form of equation 6. Furthermore, if $q = 0.5$ and $\beta_2 = \beta_1 + 2$ the symmetry $\Psi_{vol}(J) = \Psi_{vol}(\frac{1}{J})$ is obtained.

Figure A.28 illustrates the effect of varying q, and shows how it allows one to control the dominance of the expansion and shrinkage contributions. Hence for fitting purposes this formulation offers flexibility in terms of both the magnitude and the degree of strain stiffening of the response.

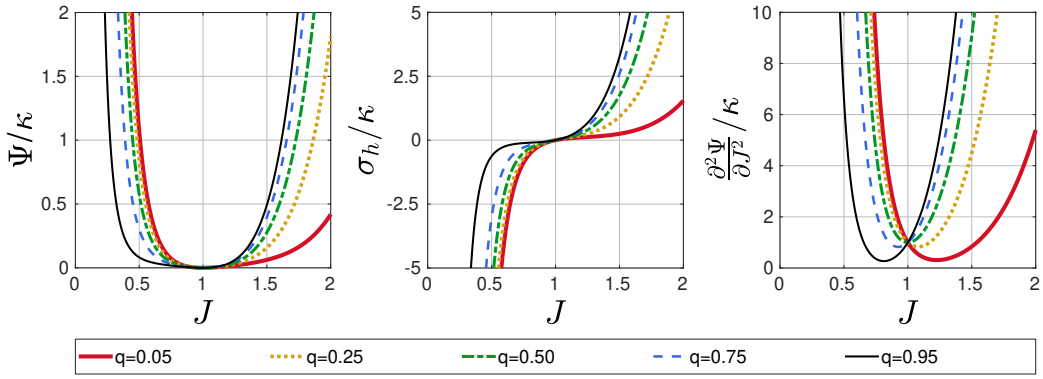

Figure A.28: The effect of q. The normalized strain energy density (left), hydrostatic stress (middle), and tangent modulus (right) for formulation 1. Curves drawn for $\kappa = 1$, $\beta_1 = 2$, $\beta_2 = 4$, $q = [0.05, 0.95]$.

However, it was found that a negative tangent may occur when q is altered to severely favour a particular domain (e.g. q close to 0 or 1) while β parameter for the "suppressed" domain is very high. This is illustrated in Figure A.29 where the combination $q = 0.05$ and $\beta_1 = 30$ (black curve in the left graph of Figure A.29), or $q = 0.95$ and $\beta_2 = 30$ (red curve in the right graph of Figure A.29), resulted in a negative tangent.

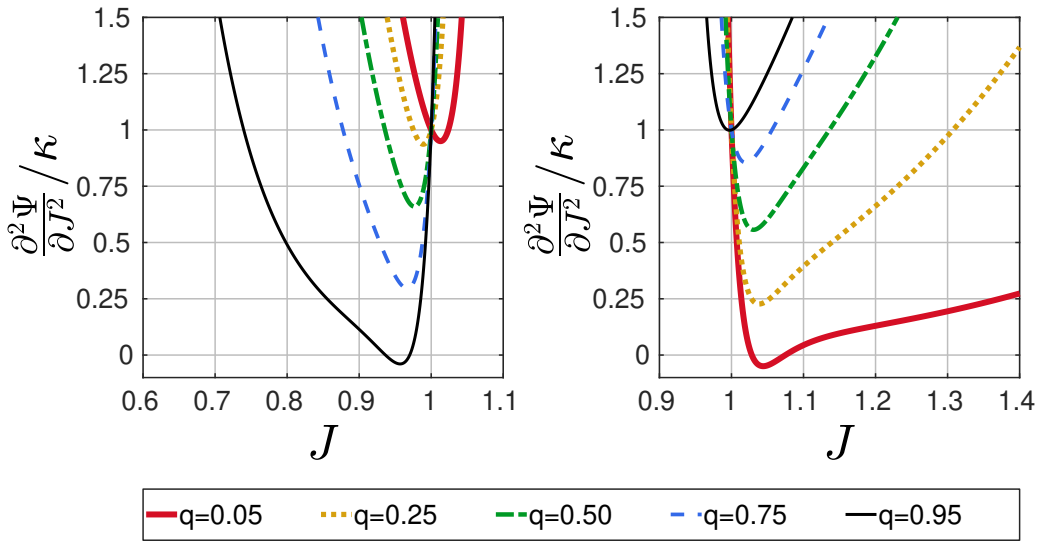

Figure A.29: The normalized tangent modulus when $\kappa = 1$, $q = [0.05, 0.95]$ and $\beta_1 = 30$, $\beta_2 = 3$ (left), or $\beta_1 = 3$, $\beta_2 = 30$ (right).

Appendix A.2. Formulation 1 with a switch statement

A second variation on formulation 1 is now presented which contains a switch statement to fully uncouple the behaviour for shrinkage and expansion:

$$\Psi_{vol}(J) = \frac{\kappa}{2} \begin{cases} \frac{1}{{\beta_1}^2}(J^{\beta_1} - 1)^2 & J \geq 1 \\ \\ \frac{1}{{\beta_2}^2}(J^{-\beta_2} - 1)^2 & J < 1 \end{cases} \tag{A.4}$$

Leading to the following expression for the hydrostatic stress:

$$\sigma_h(J) = \frac{\kappa}{J} \begin{cases} \frac{1}{\beta_1}(J^{2\beta_1} - J^{\beta_1}) & J \geq 1 \\ \\ \frac{1}{\beta_2}(J^{-2\beta_2} - J^{-\beta_2}) & J < 1 \end{cases} \tag{A.5}$$

and the tangent modulus:

$$\frac{\partial^2 \Psi_{vol}(J)}{\partial J^2} = \frac{\kappa}{J^2} \begin{cases} \frac{1}{\beta_1}\Big((2\beta_1 - 1)J^{2\beta_1} - (\beta_1 - 1)J^{\beta_1}\Big) & J \geq 1 \\ \\ \frac{1}{\beta_2}\Big((2\beta_2 + 1)J^{-2\beta_2} - (\beta_2 + 1)J^{-\beta_2}\Big) & J < 1 \end{cases} \tag{A.6}$$

This "switch-based" variation performs similarly to formulation 1 of section 4.1 but enables fully separated control of the expansion and shrinkage behaviour. Figure A.30 illustrates the effect of varying β_1 (since similar performance is obtained for β_2 these graphs are not shown here). Clearly fully independent control of strain hardening for the expansion and shrinkage domains is achieved. Furthermore, by using the conditional switch, the minimum stiffness is guaranteed to be κ and lies at $J = 1$. However, the switch-based implementation presents with a potentially undesired artefact in the form of a non-smooth transition at $J = 1$ for the tangent modulus (see the kink at $J = 1$ for the tangent graphs of Figure A.30).

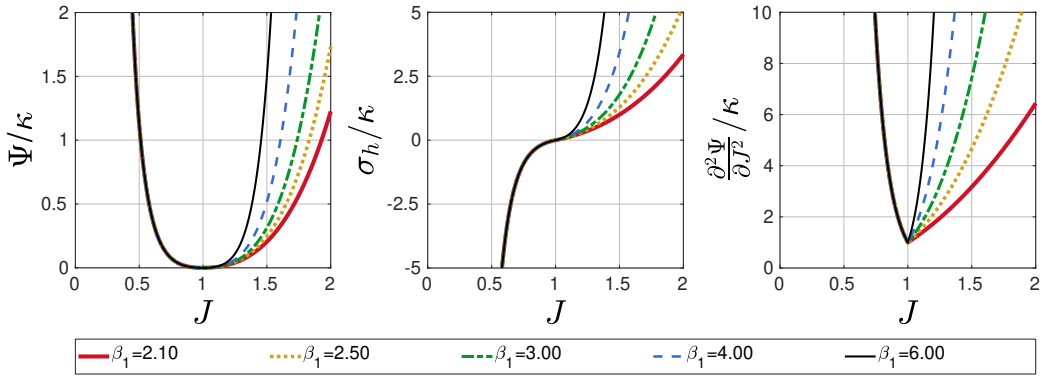

Figure A.30: The effect of β_1. The normalized strain energy density (left), hydrostatic stress (middle), and tangent modulus (right) for formulation 1. Curves drawn for $\kappa = 1$, $\beta_2 = 2$, $\beta_1 = [2.1, 6]$.

Appendix A.3. Formulation 2 without asymptote parameters

This variation is a hybrid between equation 7 and formulation 2:

$$\Psi_{vol}(J) = \kappa \begin{cases} \frac{1}{\beta_1^2}\left(\cosh\left(\beta_1(J-1)\right) - 1\right) & J \geq 1 \\ \frac{1}{2}\left[\frac{1}{\beta_2^2}\left(\cosh\left(\beta_2(J-1)\right) - 1\right) - \frac{4}{\pi^2}\ln\left(\cos\left(\frac{\pi}{2}(1+J)\right)\right)\right] & J < 1 \end{cases} \tag{A.7}$$

Resulting in the following expression for the hydrostatic stress:

$$\sigma_h(J) = \kappa \begin{cases} \frac{1}{\beta_1}\sinh\left(\beta_1(J-1)\right) & J \geq 1 \\ \frac{1}{2}\left[\frac{1}{\beta_2}\sinh\left(\beta_2(J-1)\right) - \frac{2}{\pi}\tan\left(\frac{\pi}{2}(1+J)\right)\right] & J < 1 \end{cases} \tag{A.8}$$

and the tangent:

$$\frac{\partial^2\Psi_{vol}(J)}{\partial J^2} = \kappa \begin{cases} \cosh\left(\beta_1(J-1)\right) & J \geq 1 \\ \frac{1}{2}\left[\cosh\left(\beta_2(J-1)\right) + \sec^2\left(\frac{\pi}{2}(1+J)\right)\right] & J < 1 \end{cases} \tag{A.9}$$

Here β_1 and β_2 are material parameters controlling volumetric strain-dependent stiffening. As equation A.7 shows both the shrinkage and expansion domain

feature a form equivalent to equation 7. However, to adhere to criteria V and VI of Table 1 a term similar to equation 22 (with $a(J_2 = 0)$ such that a fixed asymptote occurs at $J = 0$) is added for the shrinkage domain.

Figure A.31 and Figure A.32 illustrate the effect of varying the β_1 and β_2.

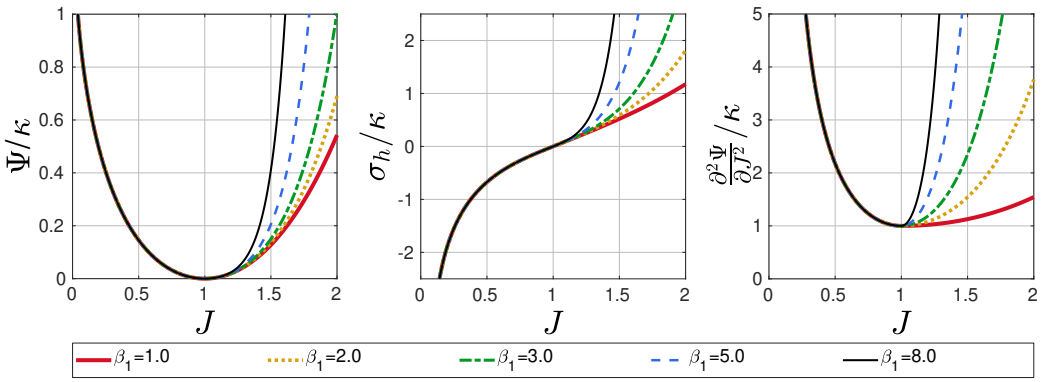

Figure A.31: The effect of β_1. The normalized strain energy density (left), hydrostatic stress (middle), and tangent modulus (right) for formulation 2. Curves drawn for $\kappa = 1$, $\beta_2 = 3$, $\beta_1 = [1, 12]$.

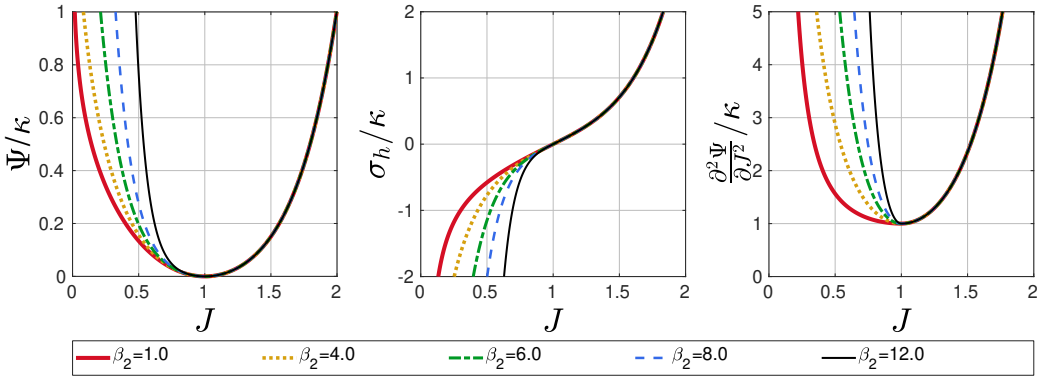

Figure A.32: The effect of β_2. The normalized strain energy density (left), hydrostatic stress (middle), and tangent modulus (right) for formulation 2. Curves drawn for $\kappa = 1$, $\beta_1 = 3$, $\beta_2 = [1, 12]$.

The graphs of Figure A.31 and Figure A.32 show fully independent control of the strain stiffening for shrinkage and expansion. This variation adheres to all criteria of Table 1. The minimum tangent occurs at $J = 1$, where,

since the third derivatives for the shrinkage and expansion terms of equation A.7 are both zero, a smooth transition occurs between the two domains.

Appendix A.4. Formulation fitting parameters

Table A.2 below presents the parameters derived from fitting presented in section 4.4.

Table A.2: Fitting parameters for formulation 1, 2 and 3 (if applicable units are MPa). Parameters for poor quality fits are not presented

id	**Data:** Bardy et al. [45] $\kappa = 0.3785$	**Data:** Petre et al. [17] $\kappa = 0.4400$	**Data:** Dart et al. [46] $\kappa = 5.051$	**Data:** Maji et al. [47] $\kappa = 11.65$
1	$\beta_2 = 0.2900$ $\beta_1 = \beta_2 + 2$	N.A.	N.A.	N.A.
2	$J_2 = 0.2544$	N.A.	N.A.	N.A.
3	$s_2 = 0.4181$ $q_2 = 0.1316$ $J_2 = 0.2643$	$s_2 = 0.04629$ $q_2 = 0.5141$ $J_2 = 0.03359$	$s_2 = 0.3577$ $q_2 = 0.8838$ $J_2 = 0.04411$	$s_2 = 0.7301$ $q_2 = 0.9981$ $J_2 = 0.4290$